Fermi National Accelerator Laboratory

TM-1603

Exploratory Orbit Analysis of TEVATRON Helical Upgrade; One: A First Look

Leo Michelotti and Selcuk Saritepe
Fermi National Accelerator Laboratory
P.O. Box 500, Batavia, Illinois

April 1989

Operated by Universities Research Association, Inc., under contract with the United States Department of Energy

Exploratory orbit analysis of Tevatron helical upgrade; One: a first look.

LEO MICHELOTTI and SELCUK SARITEPE

Anything worth doing is worth doing badly.

— Anonymous

A key feature of the Tevatron upgrade is the placement of proton and anti-proton bunches on the branches of a double helix which winds around the current closed orbit. Electrostatic separators will transfer the bunches on and off the double helix so that they experience head-on collisions only at the experimental areas, B0 and D0, all other encounters occurring at large transverse separation. In this way the number of bunches, and the luminosity, can be increased without a proportional growth in the beam-beam tune shift. The scenario raises a number of beam dynamics (*viz.* stability) issues, especially (a) the consequences of sampling magnetic fields far from the magnets' center lines, and (b) the effects of the long-range beam-beam interaction. This report presents the results of (admittedly incomplete) calculations and simulations done to date to explore (b); a Fermilab team (including Ernie Malamud, Glenn Goderre, Norman Gelfand, Gerry Jackson, and many others) have been studying (a), both experimentally and theoretically, but we shall not review those efforts here.

1 A model.

Modelling is the art of simplifying until one reaches a problem that has a chance of being solved and perhaps — dare we hope? — understood. Some of the particular simplifications made for these first calculations were:

Lattices

This report: Calculations were carried out using two low-beta (50 cm β^*) Tevatron lattices designed by Tom Collins and Karl Koepke. As a concession to the reality that accelerators are designed using SYNCH, the internal representations of the lattices were installed by reading and interpreting SYNCH output files: ATC1STEP12.OUT, provided by Karl Koepke, and PAPER.OUT;152, provided by Ernie Malamud. The former is an old (September 23, 1987) lattice with horizontal and vertical tunes placed almost exactly at 20.6; we shall refer to it as the "resonant" lattice. The latter is more recent (September 27, 1988), and its tunes are shifted slightly to $\nu_x = 20.578$ and $\nu_y = 20.590$; we shall refer to it as the "nonresonant" lattice.

The most significant simplification is the neglect of all magnetic field nonlinearities; only normal quadrupoles and bending dipoles are assumed; no field errors, no chromaticity sextupoles, no nonlinear elements of any kind were introduced into the lattices.

Future directions: The Tevatron's nonlinear fields should be added to these simulations. The tracking studies which Norman Gelfand has been doing include these effects but neglect the beam-beam interaction. Our efforts are thus complementary to his; we include beam-beam interactions but ignore field nonlinearities. The two should eventually be merged.

Electrostatic separators

This report: The locations of the twelve electrostatic separators were read from Malamud's SYNCH output file, where they appear as zero length markers. Information on their excitations was taken from a second file in Malamud's directory, CONFIG.INP, which lists the transverse kicks, in μrad, imparted by the separators. Typically, these range from a few to about 20-30 μrad.[5] Using these data the "bare" closed orbit (i.e., neglecting beam-beam interactions) was independently calculated, confirming that all four components of the closed orbit do indeed vanish at the experimental areas. (Mostly, this serves as a check that the two files were correlated correctly.)

Future directions: The PAPER.OUT and CONFIG.INP files which contain the relevant lattice and separator information have been volatile, sometimes changing on a daily basis. Some effort must be made to provide in one directory a reasonably stable set of lattices and separators with cross-referencing so that the analyst (a) knows which PAPER.OUT file corresponds to which CONFIG.INP file, and (b) has some descriptive information which identifies each lattice under study.

Bunch configuration

This report: Calculations were done using a configuration of *evenly spaced* bunches: in particular, we used a set of 21×21 bunches, as this number was both a multiple of 3, which assured collisions at both B0 and D0, and a factor of 1113, the number of available buckets.

Future directions: The actual bunch train may eventually contain more bunches and undoubtedly will possess gaps, the importance of which is that they break the symmetry, forcing us to treat each bunch individually. With gaps, each bunch experiences a different sequence of beam-beam encounters. Analyzing the existence and stability of closed orbits, as well as all the other beam dynamics effects, becomes much more complicated in such a scenario.

Beam-beam interaction

This report: The beam-beam force is essentially a space charge force but with the relativistic factor $1 - \beta^2$ replaced by $1 + \beta^2$. Montague's expression for the form of the beam-beam kick, based on a round or elliptic transverse distribution of particles, has been derived in many places, including Evans[1], Gluckstern[3], and Furman[2]. For the sake of examining a different viewpoint, a new derivation of its long-range limit is offered in Appendix A. For the calculations described in this memo, the charge distribution in each bunch was taken to be circular gaussian; given the absence of near collisions, due to the small number of bunches, using an elliptical distribution for the long-range kicks would produce little difference. All calculations were carried out using a "weak-strong" (or "large-small") approximation. There was thus a distinction between "probe" particles and "source" bunches, or macro-particles, the former having no effect on the latter. The source bunch width was recalculated at each collision site, using a nominal $\epsilon_{\rm inv} = 24\pi$ mm-mr invariant emittance throughout. In most, but not all, of the calculations the source bunches contained $N = 6 \times 10^{10}$ particles each. The relevant quantity which scales the strength of the interaction is the ratio $N/\epsilon_{\rm inv}$, usually quoted

as a small amplitude, per collision, beam-beam tune shift, as in Eq.(1) below.
Future directions: It is not obvious that the bunches are circular at B0 and D0. In addition, as will be discussed later, Montague's expression was derived assuming that probe particles travel parallel to the axis of the source bunch. This is not the case when β^* is as small as 50 cm.

Longitudinal momentum
This report: We assume the energy to be 1 TeV; the lattice contains dispersion and natural chromaticity, but it is assumed that $\delta p = 0$.
Future directions: Without a doubt, the highest priority improvement of these calculations will be to include the effect of variations in $\delta p/p$. Dispersion will change (a) the transverse position at which the probe particle crosses the source bunch, and (b) the source bunch width at the various hit locations. Chromaticity, coupled with synchrotron oscillations, may induce crossing of beam-beam resonance separatrices.

2 Linearized Dynamics

We discuss in this section results for small amplitude orbits, those which literally are infinitesimally close to the closed orbit. Exploration of moderate to large amplitude orbits will be described in the next section.

2.1 The clothed orbit

The electrostatic kicks are designed to position proton and anti-proton bunches on helical orbits while maintaining head-on collisions at B0 and D0. Over most of the ring, the separation between the two branches of the double helix is approximately 6 mm, roughly a 10σ separation for an invariant emittance of $\approx 20\pi$ mm-mr. This separation is displayed, for the nonresonant lattice, in Fig.(1). However, this "bare" orbit does not take into account the kicks arising from the long range beam-beam interaction, which distort it into a new, "clothed" orbit.[1] This is, it is hoped, a small effect, but one which may be significant if the transverse excursions of the closed orbit at the experimental areas, B0 and D0, are comparable to the transverse bunch width.

The "clothed" orbit of the model was calculated, via Newton's method, as a fixed point of the single-turn mapping. The Jacobian of the mapping, which is required by Newton's method, was automatically computed using a C++ implementation of "differential" algebra variables.[6] The resulting transverse coordinates of the "clothed" orbit at the interaction regions are shown in Figures 2 and 3. The ordinate has been scaled by the beamwidth, but this is *not* meant to imply that the effect scales accordingly; one sigma (which is about 50 μm here) is simply a useful size with which to compare the offsets. The abscissa measures λ_{sep}, the normalized strength of the separators: 0 corresponds to turning them off, and thus having no $p\bar{p}$ bunch separation; 1 corresponds to the full kicks producing the "bare" closed orbit shown in Figure 1. Notice that at B0, the motion is essentially all vertical for both lattices tested. The size of the displacement is about

[1] Not to be confused with a closed orbit calculated in LISP.

the same at both locations and smaller than 0.1σ, about 5 μm, over the full range of separator strength. For $\lambda_{sep} > 0.5$ the closed orbit distortion is already smaller than $\approx 0.02\sigma \approx 1\mu$m. These deviations are small enough so that one need not compensate for them.

The curve labelled "xpr" actually represents the normalized quantity $\alpha x + \beta x'$, and similarly for the one labelled "ypr"; the limiting value for both of these is a nominal $0.05\,\sigma$, or less. We can then solve for the limiting x'; using $\alpha = 0$ at B0, we write

$$\begin{aligned} x' &\approx 0.05\,\frac{\sigma}{\beta^*} \\ &= 0.05\,\frac{\sigma}{l}\frac{l}{\beta^*} \end{aligned}$$

where l is the bunch length. Since $l/\beta^* \approx 1$ and $4\sigma/l = (2\sigma)/(l/2) \equiv \theta_{\text{bunch}}$ is the maximum possible angle subtended by a particle passing through the 1σ region of the bunch as it passes, we get

$$x' \approx 0.01\,\theta_{\text{bunch}} \quad .$$

The angle subtended by the closed orbit of the (probe) bunch is only about 1% of the total available (source) bunch angle, which means that the closed orbit is, to an excellent approximation, parallel to the axis of the (source) bunch.

Regrettably, if we follow a similar line of reasoning for individual probe particles in the bunch, the conclusion is not as pleasant. If the probe particles are assumed to lie on an invariant phase space distribution *before* taking the beam-beam kicks into account, then it must be that at B0

$$\begin{aligned} \sigma_{x'} &= \sigma_x/\beta^* \\ &= (\sigma_x/l)(l/\beta^*) \\ &\approx \frac{1}{4}\theta_{\text{bunch}} \quad . \end{aligned}$$

β^* is so small that particles within the probe bunch are traversing the source bunch at angles that are a large fraction of θ_{bunch}, in contradiction to the basic assumption of parallel passage required for the derivation of Montague's beam-beam kick. This raises the question, which we shall not address here, of whether we need to modify the form of the beam-beam interaction for the low beta encounters.

There is one more observation of interest regarding angles. At B0, $\sigma_y \approx 50\,\mu$m and $\beta^* = 50$ cm so that $\sigma_{y'} = \sigma_y/\beta^* \approx 100\,\mu$rad. However, kicks from the separators are only $\approx 20\ \mu$rad, several times smaller than $\sigma_{y'}$ (or $\sigma_{x'}$). Naively, one would expect that such small kicks would not produce significant effects. To estimate the true effect, however, one must evaluate the kick in normalized phase space compare it to the size of the beam. The relevant quantity is the ratio,

$$\begin{aligned} \frac{\Delta(\alpha y + \beta y')}{\sigma} &= \frac{\beta \Delta y'}{\sqrt{\beta/\beta_{B0}}\,\sigma_{B0}} \\ &= \sqrt{\frac{\beta}{\beta_{B0}}} \times \frac{\Delta y'}{\sigma_{B0}/\beta_{B0}} \end{aligned}$$

$$= \sqrt{\frac{\beta}{\beta_{B0}}} \times \frac{\Delta y'}{\sigma_{y'\,B0}} \approx \sqrt{\frac{100\ \mathrm{m}}{50\ \mathrm{cm}}} \times \frac{20\ \mu\mathrm{rad}}{100\ \mu\mathrm{rad}} \approx 3$$

A kick from a single separator will translate a bunch $\approx 3\sigma$ in the appropriate (horizontal or vertical) phase space. Since the opposite bunches are kicked in the other direction, this amounts to $\approx 6\sigma$ separation in one degree of freedom, or $\approx 8\sigma$ separation in both degrees of freedom.

2.2 Beam-beam tune shift

By finding the eigenvalues of the Jacobian matrix used to calculate the "clothed" orbit we obtain as a bonus the *exact* tunes of small amplitude motion about the closed orbit. Figure (4) shows how these vary with increasing number of particles per bunch when the separators are turned off. The slope of this curve can be estimated by using the usual formula.[1]

$$\begin{aligned}
\xi &= \frac{1}{4\pi}\left(\frac{N r_p}{\gamma}\right)\left(\frac{\beta^*}{\sigma^2}\right) \\
&= \frac{1}{4\pi}\left(1.5\times 10^{-8}\,\frac{N[10^{10}]}{E[\mathrm{TeV}]}\right)\left(\frac{6\pi\times 10^6}{\epsilon_{\mathrm{inv}}[\mathrm{mm-mr}]}\cdot\sqrt{1.14}\,E[\mathrm{TeV}]\right) \\
&\approx 0.007\,N[10^{10}]/\epsilon_{\mathrm{inv}}[\pi\,\mathrm{mm-mr}] \qquad (1)
\end{aligned}$$

This expression is for a single beam-beam collision and must be multiplied by the number of encounters. For our model 21×21 configuration (i.e., 42 hits) with 10^{11} particles per bunch and $\epsilon_{\mathrm{inv}} = 24$, we get $\xi \approx 0.13$, in good agreement with the figure. The curve begins to deviate from this first order expression above 10^{11} particles per bunch, or so, indicating small interference effects among the beam-beam hits.

The tunes associated with small amplitude oscillations about the closed orbit drop rapidly as separators are turned on. In Figure 5 are plotted the eigentunes associated with the resonant lattice at 6×10^{10} and 10^{11} particles per source bunch (**ppb**); in Figure 6 are plotted the eigentunes associated with the nonresonant lattice with **ppb** $= 6\times 10^{10}$. The principal feature of these curves is their very rapid falloff, a characteristic observed in Figure 2 as well; the limiting values are attained for $\lambda_{sep} \geq 0.4-0.5$, i.e., with separators powered to $\approx$ 40-50% of their designed strength. Further, the limiting values are consistent with what one would expect from the two head-on beam-beam hits, at B0 and D0, as estimated from Eq.(1). The behavior of the eigentunes for the resonant lattice possesses an additional curious feature of no practical importance: the lower eigentunes from each pair simultaneously pass through the "bare" value of 20.6 at $\lambda_{sep} \approx 0.23$, indicating a cancellation of contributions from the separate beam-beam encounters.

NOTICE: By calculating these tunes we simultaneously have checked that the closed orbit is, in fact, linearly stable. Were this not so, the eigenvalues would not be on the unit circle.

3 Nonlinear dynamics

Going beyond the linearized model, we explored the tunes of particles on larger amplitude orbits by the simple expedient of plotting the "power" spectra obtained by evaluating FFTs of the orbits.[2] (That is, each coordinate of the orbit was treated as a "time series." In future we shall compare these with semi-analytical predictions based on a perturbative expansion of the beam-beam hits.) For example, representative spectra of the x-coordinate of an orbit, based on 4096 orbit samples, are shown in Figure 7. Prior to taking the FFT, the data were multiplied by a windowing function (the Welch window) in order to reduce the diffraction-like effects arising from a finite sample size.[9, pp.441ff] Six spectra are illustrated, corresponding to the different initial conditions appearing above each plot; the lattice was the "resonant" one obtained from Koepke. Coordinates $\underline{w} = (w_0, w_1, w_2, w_3)$ are interpreted as normalized phase space variables scaled by the bunch width: $w_0\sigma \equiv x$, $w_1\sigma \equiv \alpha_x x + \beta_x x'$, $w_2\sigma \equiv y$, and $w_3\sigma \equiv \alpha_y y + \beta_y y'$. The initial conditions shown were chosen by setting $w_1 = w_2 = w_3 = 0$ and letting w_0 ranging from 0.50 to 3.00; **ppb** is fixed at 7×10^{10}, and $\lambda_{sep} = 0$. These spectra are very clean, exhibiting a single prominent peak which shifts downward with increasing amplitude. Notice, however, that secondary frequencies begin to grow in influence at the largest amplitudes. We shall return to this later.

If we now plot the position of these peaks as a function of **ppb** for these same six initial conditions we obtain the curves displayed in Figure 8. The top curve, which has been appended to the set and corresponds to $w_0 = 0.01$, is virtually identical with the one appearing in Figure 4, thereby confirming the previous calculation (or the present ones, depending on one's stronger insecurities). The result of slicing these data the other way and plotting tune versus w_0 for a fixed **ppb** $= 6 \times 10^{10}$, is shown as the top curve in Figure 9. If we now power the separators we obtain the other curves in this figure; included are two cases from the nonresonant lattice, for comparison. (**Note: sc** $= \lambda_{sep}$) The very strong amplitude dependence of the tune is effectively wiped out by powering the separators. The small effect which remains is seen more easily in Figure 10, where the scale has been expanded. (Another calculation in the works: a comparison of this figure with the expectations of perturbation theory.)

Finally, we explored a collection of orbits at both moderate and large amplitudes using the EOA (Exploratory Orbit Analysis) graphics shell AESOP.[7] We shall describe a few of these here, but static, two-dimensional pictures do not convey the full experience of viewing these orbits as they develop in (projected) four dimensions. Accordingly, some of these "experiments" have been electronically logged into "fables" which can be accessed from any user area in Accelerator Division's ALMOND cluster by:

(1) Logging into ALMOND on the Evans and Sutherland PS390 terminal located in the High Bay Mezzanine area of the Cross-Gallery.

(2) At DCL level, enter $ RUN USR$DISK4:[MICHELOTT.AESOP.PUBLIC.HELIX]AESOP

(3) Choose the archival option from the menu that AESOP presents. When the next menu pops up, choose to read data from a file.

[2] An eminent nonlinear dynamicist has stated recently that Fourier transforms are little more than a refuge for the incompetent. This was meant to emphasize that the transform is a linear filter, appropriate to linear problems.

(4) AESOP will ask you for the file name. Three are currently available:
USR$DISK4:[MICHELOTT.AESOP.PUBLIC.HELIX]FABLE_n.DAT, where n is 1, 2, or 3.

(5) AESOP will tell you the "fable" behinds the orbit that you are about to view. (Rather than dwell on the negative connotation of a fable as a story of questionable veracity, I prefer to think of it as one which is designed to teach a lesson.) When it prompts that it is ready to draw an orbit, simply type "OK," or any other friendly response, and a carriage return. The top four dials of the PS390's dial box can be used to change the viewing angle of the display and to boost the "gain" on the data. (More bells and whistles will be added in the fullness of time.)

(6) When the fable is finished, you can view AESOP's main menu once more by entering a 0 at the prompt. When trouble arises, or for further instructions in general, see me (LM).

An effective "screen dump" is also available which creates a PostScript file of the display which can be printed on our new QMS printer; again, see me (LM) for details.

A few representative runs at moderate amplitudes are logged in Figures 11 through 13. Each figure tracks the behavior of an orbit passing through a given point in phase space as λ_{sep}, the normalized separator strength, increases from 0 to 0.5; **ppb** was set at 10^{11} for Figures 11 and 12 but decreased to 7×10^{10} in Figure 13; the calculations for these figures were carried out using the nonresonant lattice. For each value of λ_{sep} we display four phase space projections of the (four-dimensional) orbit and the spectra for horizontal and vertical coordinates. The two-dimensional projections are along the horizontal, (w_0, w_1), and the vertical, (w_2, w_3), coordinates. The coordinates for the three dimensional projections, which we shall refer to as $\delta\delta I$ plots, are the horizontal and vertical "angle" variables and an "action" variable, horizontal action in the left hand plots and vertical in the right. These variables are those obtained by expressing the two-dimensional projections in polar coordinates rather than Cartesian, actions being equivalent to radius squared.

As you scan through Figure 11a-f notice the change from clean, smooth KAM tori when $\lambda_{sep} \leq 0.2$ — by accident, the orbit starts out very close to a stable resonant orbit, which would appear as a line — through a chaotic layer for $\lambda_{sep} \approx 0.3$, and returning to regular behavior when $\lambda_{sep} \geq 0.4$. Observe the increasing complexity of the power spectra as λ_{sep} increases and the orbit approaches a chaotic condition. This broadband "noise" is typical of chaotic behavior. Conversely, as the chaotic layer passes the orbit and it settles down to smooth torus once again, the spectrum becomes once more discrete.[3] The orbits in Figure 12 behave similarly. Interestingly, the orbit in Figure 12 passes through a mildly chaotic layer for $\lambda_{sep} \approx 0.1$, quiets down at $\lambda_{sep} = 0.2$, before hitting the "expected" chaotic layer at $\lambda_{sep} = 0.3$. One *very* intriguing feature emerges when you compare the spectra from all three figures. Notice that the peak spectral component shifts with increasing λ_{sep}, as is reasonable, and that the chaotic layer at $\lambda_{sep} = 0.3$ is correlated with (a) the peak spectral component hitting the value 0.6 and (b) a second strong, noisy spectral component coming into existence at 0.8. This suggests a locking onto the $\nu_x = \nu_y = 3/5$ resonance separatrix as the mechanism of chaos, with a possible interference from the $\nu_x = \nu_y = 4/5$ or $2/5$ separatrix as well.

Finally in Figure 14 we see what happens to a "moderate amplitude" orbit when **ppb** is pushed up to

[3] I am curious about how these orbits would "sound" if we could convert these spectra into audible sound waves. Is it possible that the ear could discriminate between chaotic and regular behavior better than the eye?

2×10^{11}. This is admittedly large, but think of decreasing the invariant emittance by a factor of four or five and the effect is the same. By accident we found an orbit which begins very close to a periodic orbit, corresponding to a double resonance: $\nu_x = \nu_y = 0.75$. The broadband noise in the spectrum is very strong, but even here the orbit quiets down when $\lambda_{sep} \geq 0.5$. Overall, these explorations corroborate the conclusion of the tangential calculations that long-range beam-beam effects on moderate amplitude orbits tend to die out at $\lambda_{sep} \approx 0.5$.

However, large amplitude orbits can experience a different phenomenon, one which is best described in textilic terms: what happens is as though KAM tori were literally woven from threads which unravel and become entangled.[4] To see this happening, we shall track the behavior of the orbit passing through $\underline{w} = (3, 0, 0, 3)$ as the normalized separator strength, λ_{sep}, is increased from 0.0 to 0.5. This set of calculations were carried out using the resonant lattice. The corresponding $\delta\delta I$ plots are shown in Figure 15. The first plot shows a separatrix for $\lambda_{sep} = 0$; **ppb** has been set to 10^{11}; those who think this is too large can rescale by decreasing ϵ_{inv}. The orbit, which is in the vicinity of a $2\nu_x - 2\nu_y$ separatrix, is chaotic and visits both sides of the separatrix. (Bear in mind that what we are viewing is only one three-dimensional slice through the full separatrix.) A remarkable transition occurs as λ_{sep} increases from 0.0 to 0.1; Figure(15b) shows the orbit at $\lambda_{sep} = 0.1$. The separatrix now contains only two lobes rather than the four that it previously had; it looks more like a $\nu_x - \nu_y$ separatrix. It is almost as though one of the unstable resonant orbits defining the separatrix has undergone a transition to stability. (Are we observing here some four-dimensional form of period doubling?) At $\lambda_{sep} \approx 0.14$ another remarkable jump occurs, and the orbit fills the wedge formed by the separatrix, as seen in Figure (15c). The "wedge" smooths out and becomes tighter until, at $\lambda_{sep} \approx 0.3$, as seen in Figure (15d), it winds around a tight KAM torus, close to a stable resonant orbit. (Note the change in viewing angle.) Although it is difficult to tell from these figures, this torus lies remarkably precisely in the intersection region of the separatrix of Figure(15b) or, equivalently, at the cusp of the wedge in Figure (15c). If we now increase λ_{sep} further, an extraordinary thing happens: the torus gets larger and *begins to unravel.* This is seen in Figure(15e), which shows the orbit at $\lambda_{sep} = 0.4$. The unravelling has begun, but enough of shape of the torus remains that one can make out its former existence and location. By $\lambda_{sep} = 0.5$ the torus has completely disappeared and the orbit is simply a tangled thread, as seen in Figure(15e). A stereo pair of this same orbit (with many more samples) is displayed in Figure 16 for those who can control their eyes sufficiently to observe the 3D effect. Here we have a phenomenon due to the long range beam-beam interaction which does not vanish for $\lambda_{sep} > 0.5$. These very large amplitude orbits are still feeling the effect of the source bunches. Keep in mind, however, that we have displayed only the orbits passing through one particular point in phase space. Not all large amplitude orbits behave like this. Indeed, the orbit passing through $(3, 0, 0, -3)$ still lies on an identifiable, perfectly regular torus. Thus, the problem is (a) to identify the probability of actually encountering such orbits, and (b) understand their impact on stability. This particular tangled orbit, for example remained bounded for over 50,000 iterations. Though it looks ugly, this aesthetic judgement may have no relevance to issues of stability.

Some large amplitude orbits whose tunes are near resonance exhibit phaselock, a phenomenon frequently associated with coupled resonant systems. This is seen, for example, in Figure 17. This orbit (belonging to the resonant lattice) spends most of its history with horizontal and vertical phases locked near $\delta_1 - \delta_2 \approx 0$, or π,

[4] Don Edwards has offered an alternative, culinary metaphor: the "lasagna" of nested KAM tori gives way to a "spaghetti" of tangled orbits.

resulting in the vertical walls appearing in the $\delta\delta I$ projections. The transitions between these two walls take place on time scales small compared to the time spent in the locked regions. To lowest order, and under suitable assumptions, the distribution of particles in phase space is nearly invariant under this convective churning. The "suitable" assumptions are that (1) $\beta_x = \beta_y$ at B0, (2) $\sigma_x = \sigma_y$ at B0, and (3) the bare (i.e., in the absence of beam-beam interaction) distribution is an invariant Gaussian. This last means, for example, that the (x, x') probability measure over phase space can be written,

$$\begin{aligned} d\mu &= e^{-x^2/2\sigma_x^2}\, e^{-x'^2/2\sigma_{x'}^2}\, dx dx' \\ &= e^{-\beta_x I_x/\sigma_x^2}\, dI_x d\delta_x \quad , \end{aligned}$$

since $\sigma_{x'} = \sigma_x/\beta^*$. After integrating over angles, the distribution measure over both degrees of freedom is

$$d\mu = exp\left[-\beta^*(I_x + I_y)/\sigma^2\right]\, dI_x dI_y$$

However, $I_x + I_y$ is a dynamical invariant (constant of motion) for the $2\nu_x - 2\nu_y$ resonance. Therefore, level surfaces of the distribution function are invariant surfaces of the dynamical system, which means that the distribution function itself will remain invariant.

References

[1] Lynn R. Evans. *The Beam-Beam Interaction.* Technical Report, European Organization for Nuclear Research, 1983. CERN SPS/83-38.

[2] Miguel A. Furman. *Practical Approximations for the Electric Field of Elliptical Beams.* Technical Report, Lawrence Berkeley Laboratory, 1987. SSC-N-312.

[3] Robert Gluckstern. *Scalar Potential for Charge Distributions with Ellipsoidal Symmetry.* Technical Report, Fermi National Accelerator Laboratory, 1986. Fermilab TM-1402.

[4] John David Jackson. *Classical Electrodynamics.* John Wiley & Sons, New York.

[5] Ernie Malamud. An electrostatic separator scheme for the tevatron. September 1, 1987 (unpublished).

[6] Leo Michelotti. Differential algebras without differentials: an easy c++ implementation. This Conference.

[7] Leo Michelotti. Exploratory orbit analysis. This Conference.

[8] B. W. Montague. October 1968. CERN ISR/68-38.

[9] William H. Press, Brian P. Flannery, Saul A. Teukolsky, and William T. Vettering. *Numerical Recipes in C.* Cambridge University Press, New York, 1988.

A The long range beam beam kick

Montague [8] is generally credited with having first written the integral representation for the potential due to a set of line charges with Gaussian transverse distribution,

$$U = \lambda \int_0^\infty dt \frac{\exp\left[-\frac{1}{2}\left(\frac{x^2}{t+\sigma_x^2} + \frac{y^2}{t+\sigma_y^2}\right)\right]}{\sqrt{(t+\sigma_x^2)(t+\sigma_y^2)}}$$

although he himself gives the credit to a colleague, one Houssais. This expression was recently rederived by Gluckstern.[3] The integral is logarithmically divergent, as it must be: one cannot escape the potential well of an infinitely long line charge. One way of getting around this would be to reduce the range of the field by giving the photon a small mass, m. Furman [2] points out that the potential then would contain a $\ln m$ term, and attributes the divergence to the limit $m \to 0$.

The infinite potential is not a real problem, however, since we really need only the electric field, which is finite. When $\sigma_x = \sigma_y \equiv \sigma$, the transverse electric field takes the form

$$E(r) = 2\lambda(1 - e^{-r^2/2\sigma^2})/r \quad ,$$

with $r^2 = x^2 + y^2$. This can be obtained directly from the Montague's potential or derived more easily using Gauss's law.

The beam-beam force is obtained from the electrostatic field by Lorentz transformation. Finite length of a bunch is incorporated by turning fields on and off at the passage of its ends, an approximation partially justified by the fact that the electromagnetic field of a particle travelling near the speed of light is squeezed into a small transverse angle.

The electrostatic field is computed, of course, in the rest frame of the source bunch. However, consider viewing a beam-beam collision in the Lorentz frame in which a proton bunch is at rest as it passes B0. What actually happens is an example of the classic "train in the tunnel" problem. We shall take the bunch length to be ≈ 50 cm and relativistic $\gamma \approx 1000$ in the (Fermi)lab frame. What we see is ***not*** a proton bunch of length 500 m: B0 itself is only 8 cm long in this frame, the anti-proton bunch is about 0.3 mm long, and the Tevatron itself is an ellipse with a 1 m semi-minor axis. The 500 m long string of protons at rest which appears in Montague's expression is actually laid out 8 cm at a time, much like a scroll being unrolled on one side and rolled up on the other. Orbits of individual protons look like pieces of a cycloid, with an added delay that allows B0 to pass. Does this matter? Does it matter at other points in the ring where the transverse separation can be as much as 6 mm? We assume for now that it does not and continue.

As an exercise, we shall obtain the long range part of Montague's kick by directly integrating the impulse from a relativistic point charge. Directly from Jackson[4, Eq.(11.118)], the transverse field due to a point macro-particle moving with velocity v is

$$E_\perp = \frac{\gamma Q b}{(b^2 + \gamma^2 v^2 t^2)^{3/2}}$$

where $t = 0$ at the instant of closest passage to the observation point, Q is the charge of the macro-particle, b is the impact parameter, and $\gamma^2(1 - v^2/c^2) = 1$. This is written in cgs units; to convert to rationalized mks, replace Q with $Q/2\pi\epsilon_o$. The integrated impulse felt by a motionless test charge, q, is given by

$$\begin{aligned}
\Delta p_\perp &= q \times \int_{-\infty}^{\infty} dt E_\perp(t) \\
&= (\gamma Q q b) \times \frac{1}{b^2} \frac{t}{(b^2 + \gamma^2 v^2 t^2)^{1/2}} \Bigg|_{t=-\infty}^{\infty} \\
&= \frac{2Qq}{b v_{\rm rf}}
\end{aligned}$$

I have appended the subscript "rf" to v to emphasize that this is the velocity in the rest frame of the "probe" particle. In the (Fermi)lab frame, both the probe and the source are travelling with the same velocity, $v_{\rm lab}$, but in opposite directions, so that

$$v_{\rm rf} = \frac{2v_{\rm lab}}{1 + (v_{\rm lab}/c)^2} \quad . \tag{A2}$$

If the source is a bunch of N protons and the probe is a single antiproton, or vice versa, then the product $Qq = -Ne^2$.

We now calculate the "kick," $\Delta x'$, imparted to the probe. First note that we can equate the transverse impulse as seen in both frames.

$$\begin{aligned}
(\Delta p_\perp)_{\rm rf} &= (\Delta p_\perp)_{\rm lab} \\
&= \Delta(\gamma m v_\perp)_{\rm lab} \\
&\approx \gamma m (\Delta v_\perp)_{\rm lab}
\end{aligned}$$

Here I have neglected terms of order $\Delta\gamma/\gamma$; m is the mass of a *single* proton. What we really want is $\Delta x'$.

$$\begin{aligned}
x' &= \frac{dx}{ds} = \frac{dx}{dt}\frac{dt}{ds} = \frac{1}{\beta c} v_\perp \\
\Delta x' &= \frac{1}{\beta c} (\Delta v_\perp)_{\rm lab} \\
&= \frac{1}{\beta c \gamma m} (\Delta p_\perp)_{\rm rf} \\
&= -\frac{1}{mc\beta\gamma} \frac{2Ne^2}{b v_{\rm rf}} \\
&= -\frac{N r_p}{\gamma b} (1 + 1/\beta^2)
\end{aligned}$$

where I have substituted the classical proton radius $r_p = e^2/mc^2$, so that we no longer have to worry about the difference between cgs and radionalized mks units. This is written as a scalar equation; to write it in two-dimensional transverse space, simply replace $1/b \leftarrow \underline{x}/|\underline{x}|^2$; To write out the full beam-beam kick, of

which this is the long-range limit, replace $1/b \leftarrow \left(1 - e^{-|\underline{x}|^2/2\sigma^2}\right) \underline{x}/|\underline{x}|^2$.

$$\Delta\underline{x}' = -\frac{N r_p}{\gamma}\,(1 + 1/\beta^2)\,\left(1 - e^{-|\underline{x}|^2/2\sigma^2}\right)\,\frac{\underline{x}}{|\underline{x}|^2} \tag{A3}$$

Putting in the units, we obtain

$$\begin{aligned}
\Delta\underline{x}'\,[10^{-8}] &= -2.9\,(1+\varepsilon)\,\frac{N\,[10^{10}]}{E\,[\mathrm{TeV}]}\,\left(1 - e^{-|\underline{x}|^2/2\sigma^2}\right)\,\frac{\underline{x}}{|\underline{x}|^2}\,[\mathrm{mm}^{-1}] \\
\varepsilon &= \frac{1}{2}(1 + 1/\beta^2) - 1 \\
&= \frac{1}{2}\,\frac{1}{\gamma^2 - 1} = \frac{1}{2}\,\frac{1}{1.14(E\,[\mathrm{GeV}])^2 - 1}
\end{aligned}$$

These are small kicks: the maximum possible value occurs during a head-on collision at B0. If I assume that $E\,[\mathrm{TeV}] = 0.8$, $N\,[10^{10}] = 6$, and $\sigma = 50\mu\mathrm{m}$, then $|\Delta\underline{x}'| \leq 2\mu\mathrm{rad}$. A long-range beam-beam kick at a distance of 6 mm will be about 2% of this, or $\approx 0.04\ \mu\mathrm{rad}$. For comparison, the kick arising from field errors in a Tevatron dipole (at one inch) is on the order of $0.8\ \mu\mathrm{rad}$.

Because the probe is in a source-free region during a long range beam-beam kick, the interaction can be thought of as due to a vector potential $A_3(\underline{x}, \theta)$, whose relationship to the kick is given by,

$$\begin{aligned}
\Delta\underline{x}'(\underline{x}) &= -\partial U(\underline{x})/\partial\underline{x} \\
A_3(\underline{x}, \theta) &\equiv -\frac{|B\rho|}{R}\,U(\underline{x})\,\delta_{\mathrm{per}}(\theta - \theta_{\mathrm{o}}) \\
\delta_{\mathrm{per}}(\theta - \theta_{\mathrm{o}}) &= \sum_{n=-\infty}^{\infty} \delta(\theta - \theta_{\mathrm{o}} + 2\pi n)
\end{aligned}$$

Further, if we expand $\underline{x}$ about the transverse beam-beam separation, $\underline{x}_{\mathrm{o}}$ — say $\underline{x} = \underline{x}_{\mathrm{o}} + \underline{u}$ with $\|\ \underline{u}\ \| \ll \|\ \underline{x}\ \|$ — then we can easily identify the equivalent field multipoles. Let the horizontal and vertical components of $\underline{u}$ be (u_1, u_2) and define the associated complex variable u to be $u = u_1 + iu_2$, in the usual way. The multipole expansion of A_3 is written,

$$\begin{aligned}
A_3(\underline{x}_{\mathrm{o}} + \underline{u}, \theta) &= -B_{\mathrm{o}}\mathrm{Re}\left[\sum_{n=1}^{\infty} \frac{1}{n} c_{n-1} u^n\right] \\
c_n(\underline{x}_{\mathrm{o}}, \theta) &= (b_n + ia_n)_{(\underline{x}_{\mathrm{o}}, \theta)}
\end{aligned}$$

We then proceed with the following line of development.

$$\begin{aligned}
-\partial U(\underline{x})/\partial\underline{x}\ \delta_{\mathrm{per}}(\theta - \theta_{\mathrm{o}}) &= -\partial U(\underline{x}_{\mathrm{o}} + \underline{u})/\partial\underline{u}\ \delta_{\mathrm{per}}(\theta - \theta_{\mathrm{o}}) \\
&= -\frac{B_o R}{|B\rho|}\left(\frac{\partial}{\partial u_1}, \frac{\partial}{\partial u_2}\right)\ \mathrm{Re}\left[\sum_{n=1}^{\infty} \frac{1}{n} c_{n-1} u^n\right]
\end{aligned}$$

$$
\begin{aligned}
&= -\frac{B_o R}{|B\rho|}\mathrm{Re}\left[\left(\frac{d}{du}, i\frac{d}{du}\right)\sum_{n=1}^{\infty}\frac{1}{n}c_{n-1}u^n\right] \\
&= -\frac{B_o R}{|B\rho|}\mathrm{Re}\left[(1,i)\sum_{n=0}^{\infty}c_n u^n\right] \\
&= -\frac{B_o R}{|B\rho|}(\mathrm{Re}, -\mathrm{Im})\sum_{n=0}^{\infty}c_n u^n \\
&= -\frac{B_o R}{|B\rho|}\sum_{n=0}^{\infty}c_n^* u^{*n}
\end{aligned}
$$

We similarly expand Eq.(A3) but now viewed as a relation between complex variables.

$$
\begin{aligned}
\Delta x' &= -\frac{N r_p}{\gamma}(1+1/\beta^2)\frac{x_o + u}{|x_o + u|^2} \\
&= \frac{N r_p}{\gamma}(1+1/\beta^2)\sum_{n=0}^{\infty}\left(\frac{-1}{x_o^*}\right)^{n+1} u^{*n}
\end{aligned}
$$

These two expressions now enable us to identify the equivalent integrated multipoles strengths.

$$
\frac{B_o R}{|B\rho|}\int d\theta(\, b_n + i a_n\,) = -\frac{N r_p}{\gamma}(1+1/\beta^2)\left(\frac{-1}{x_o}\right)^{n+1}
$$

We record here for convenience:

$$
\frac{N r_p}{\gamma}(1+1/\beta^2)\ [\mathrm{meters}] = 2.9\times 10^{-11}(1+\varepsilon)\frac{N\,[10^{10}]}{E\,[\mathrm{TeV}]}
$$

B FONCRA

We can crudely estimate the contribution of the long range beam-beam interactions to resonance widths by doing a first order, naive, conservative resonance analysis. (FONCRA) It is

first order in that we calculate resonance contributions only to first order in perturbation theory.

naive [1] because we calculate only the contribution of the lowest possible multipole to each resonance.

conservative because we will neglect the benign effect of shear terms, which tend to diminsh the effect of resonances.

The argument goes as follows. Near a resonance, the Hamiltonian of the system is approximated by the one-dimensional resonance form,

$$\begin{aligned} K &\approx (\underline{m}\cdot\underline{\nu}+n)\,J + 2\mathrm{Re}[\,G\exp i(\underline{m}\cdot\underline{\delta})\,]I_1^{m_1/2}I_2^{m_2/2} \\ J &= \underline{m}\cdot\underline{I}/\,\|\,\underline{m}\,\| \end{aligned} \qquad (\text{B1})$$

Here, $I = (\,I_1, I_2\,)$ and $\delta = (\,\delta_1, \delta_2\,)$ are "amplitude-phase" variables defined with respect to linear motion about the closed orbit. Their relationship to the ordinary phase space variables x and x' is given by the following (subscript suppressed).

$$\begin{pmatrix} x \\ \alpha x + \beta x' \end{pmatrix} = \sqrt{2\beta I}\begin{pmatrix} \sin(\tilde{\psi}+\delta) \\ \cos(\tilde{\psi}+\delta) \end{pmatrix}$$

Here, $\tilde{\psi} \equiv \psi - \nu\theta$. The value of the factor $\Delta \equiv \underline{m}\cdot\underline{\nu}+n$, which appears in the first term of Eq.(B1), measures the (signed) distance to the resonance line $\underline{m}\cdot\underline{\nu}+n=0$ in tune space. Finally, the resonance coupling constant, G, is a linear functional of a multipole distribution function.

$$\begin{aligned} G &= (-i/\sqrt{2})^{m_1+m_2}\,\frac{1}{m_1+m_2}\begin{pmatrix} m_1+m_2 \\ m_1 \end{pmatrix}\frac{B_oR}{|B\rho|} \\ &\quad\times\int\frac{d\theta}{2\pi}\left\{\begin{array}{l} (-1)^{m_2/2}b_{m_1+m_2-1} \\ (-1)^{(m_2+1)/2}a_{m_1+m_2-1} \end{array}\right\}\beta_1^{m_1/2}(\theta)\beta_2^{m_2/2}(\theta)\exp i[\underline{m}\cdot\underline{\tilde{\psi}}-n\theta] \end{aligned}$$

The normal (skew) multipole is chosen for even (odd) m_2.

The important consideration is this: how does the second term in Eq.(B1) compare to the first? If the first is dominant, then the working point is far enough from this resonance so that it will not influence the motion appreciably; if the second is comparable to the first, then we are within its region of influence. Let us denote the typical "scale" of a variable v by the symbol $\lfloor v \rceil$. The relevant quantity is then

$$\Delta_{crit} \equiv \lfloor G \rceil \lfloor I \rceil^{\frac{M}{2}-1} \quad ,$$

[1] It may not be too pessimistic, but it would be definitely uncharitable, to change this to W, for "Wrong," in the acronym.

where $M \equiv m_1 + m_2$. This number provides a crude estimate of the "resonance width" in tune space: the resonance is influential for $\Delta \leq \Delta_{crit}$.

We now estimate the contribution from the long range beam-beam hits. Using the results of Appendix A,

$$\lfloor b_{M-1}, a_{M-1} \rceil \approx 2.9 \times 10^{-11}\text{m}\ (N[10^{10}]/E[\text{TeV}])\ (1/d)^M \quad ,$$

$M = m_1 + m_2$, and the asymptotic expression,

$$\begin{pmatrix} M \\ m_1 \end{pmatrix} \leq \begin{pmatrix} M \\ M/2 \end{pmatrix} \approx 2^{M+1}/\sqrt{2\pi M} \quad ,$$

we get the estimate

$$\Delta_{crit} \leq \left(2.9 \times 10^{-11}/\lfloor I \rceil\right) \times \left(\sqrt{2\lfloor \beta \rceil \lfloor I \rceil}/\lfloor d \rceil\right)^M \times \sqrt{\frac{2}{\pi M^3}} \quad .$$

Note that all length scales are to be expressed in meters. Thus, the FONCRA resonance widths decrease exponentially with order, M, according to a base of $\sqrt{2\lfloor \beta \rceil \lfloor I \rceil}/\lfloor d \rceil \approx \sigma/d$.

Finally, we approximate

$$\begin{aligned} [I] &\approx \frac{1}{2\pi}\left(10\pi \times 10^{-6}\right)\frac{1}{800} \\ &\approx 0.6 \times 10^{-8}\ \text{m} \\ \sqrt{\beta_1\beta_2} &\approx 100\ \text{m} \\ d &\approx 6\ \text{mm} = 6 \times 10^{-3}\ \text{m} \\ N/E &\approx 1 \end{aligned}$$

and even more conservatively neglect the factor $\sqrt{2/\pi M^3}$ to get

$$\Delta_{crit} \leq 0.005 \times (0.1)^M$$

The small size of these numbers suggest that the long range beam-beam hits will not of themselves contribute significantly to the widths of sum resonances.

FIGURE CAPTIONS

Figure 1: Orbit separation for the models' design closed orbits: (a) resonant lattice (point at B0 suppressed), and (b) non-resonant lattice.

Figure 2: The "clothed" orbit at B0 as a function of normalized separator strength: (a) resonant lattice, and (b) non-resonant lattice. The lines labelled **xpr** and **ypr** refer to x' and y', respectively.

Figure 3: The "clothed" orbit at D0: as a function of normalized separator strength: (a) resonant lattice, and (b) non-resonant lattice.

Figure 4: Calculated tunes of small amplitude motion with separators turned off as a function of bunch intensity. (21×21 configuration) These tunes begin to fall slightly below the linear, incoherent prediction of $0.007N/\epsilon$ only for bunch intensities in excess of 10^{11}.

Figure 5: Effect of increasing bunch separation on tune shifts: resonant lattice.

Figure 6: Effect of increasing bunch separation on tune shifts: nonresonant lattice.

Figure 7: FFT spectra of orbits at moderate amplitudes.

Figure 8: Tune versus bunch intensity for a variety of initial conditions and with separators off. Unlike the tunes displayed in Figure 4, these tunes were obtained by (fast) Fourier transforming tracking "data," spectra of which were illustrated in Figure 7, and plotting the peak values. The top curve agrees with that in Figure 4, as it should.

Figure 9: Tune versus initial amplitude for fixed **ppb**: resonant lattice. This is an orthogonal slice through the data of the previous figure.

Figure 10: Tune versus initial amplitude; nonresonant lattice; blown up scale.

Figure 11: AESOP projections and tune spectra for an orbit of "moderate amplitude." The initial conditions are held fixed at the values shown in the upper-left corner of each picture; the normalized separator strength increases in going from the first frame to the last. Passage through a chaotic layer, usually at a separator strength of 0.3, is recognized by both the non-surface like character of the AESOP plot and the simultaneously "noisy" character of the frequency spectrum.

Figure 12: A second example of the behavior of a moderate amplitude as a function of separator strength.

Figure 13: The null figure.

FIGURE CAPTIONS (cont.)

Figure 14: Illustration of an orbit at larger amplitude and with greater bunch intensity.

Figure 15: As tori unravel, orbits become "tangled." Is this a new class of particle motion? It is certainly not expected from intuition built up from experience with two-dimensional (one degree of freedom) systems.

Figure 16: A stereo pair providing a three dimensional illustration of a tangled orbit for those who can cross their eyes without defocussing and not faint.

Figure 17: An orbit exhibiting phaselock, a phenomenon frequently occurring in regions of the phase space of a two degree-of-freedom resonance.

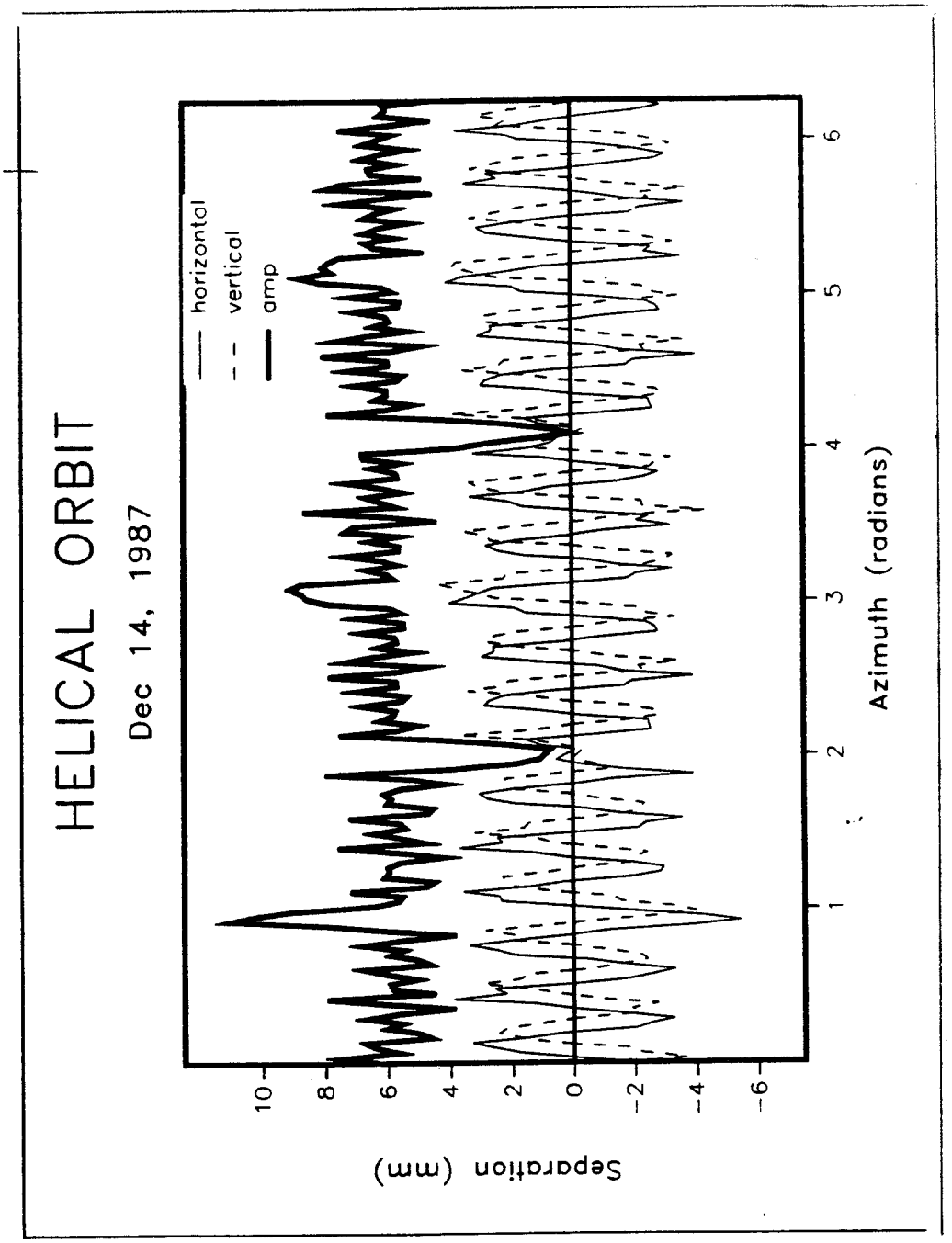
HELICAL ORBIT
Dec 14, 1987
horizontal
vertical
amp
Separation (mm)
10
8
6
4
2
0
-2
-4
-6
1
2
3
4
5
6
Azimuth (radians)

Figure 1(a)

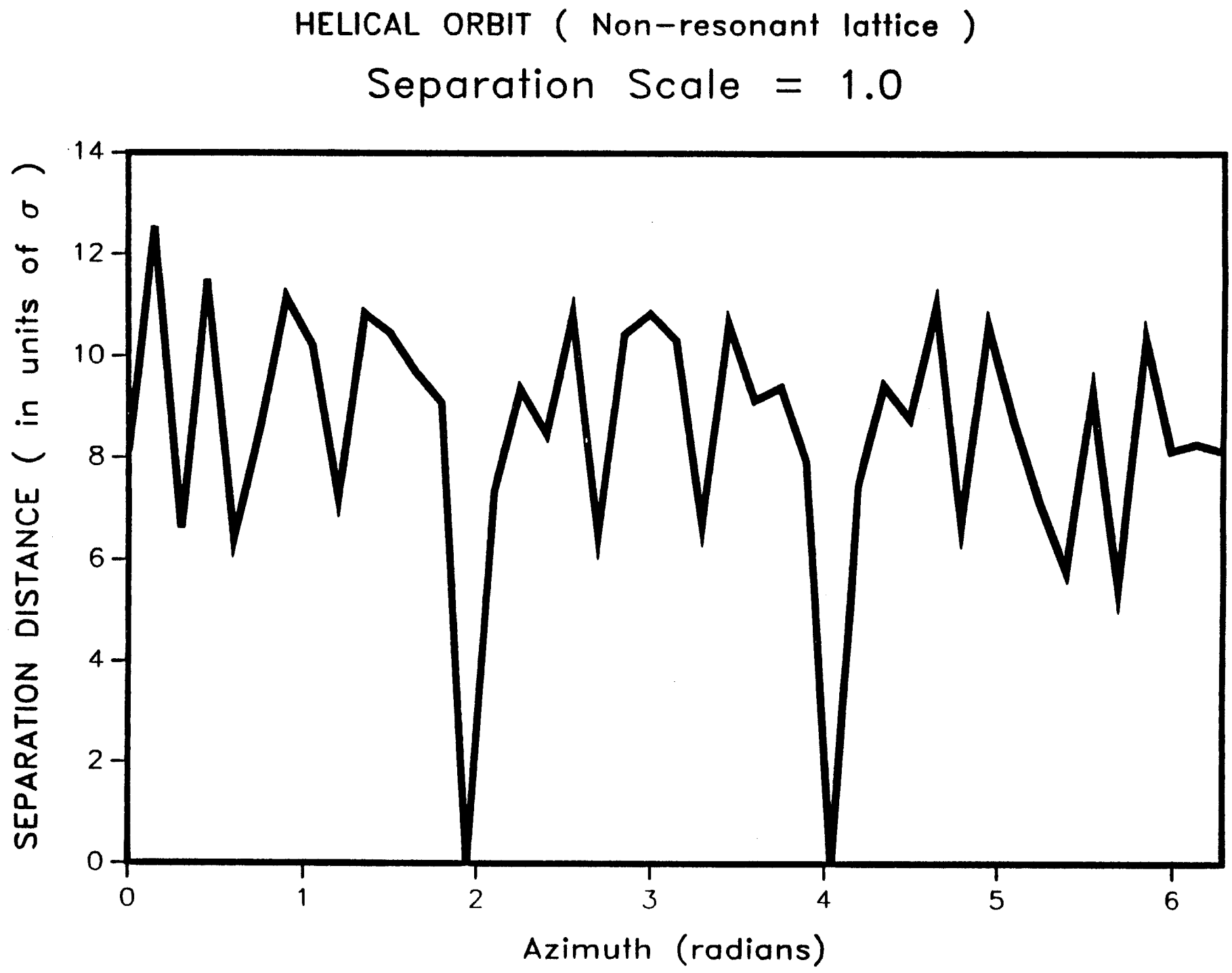
HELICAL ORBIT (Non-resonant lattice)
Separation Scale = 1.0
SEPARATION DISTANCE (in units of σ)
0
2
4
6
8
10
12
14
0
1
2
3
4
5
6
Azimuth (radians)

Figure 1(b)

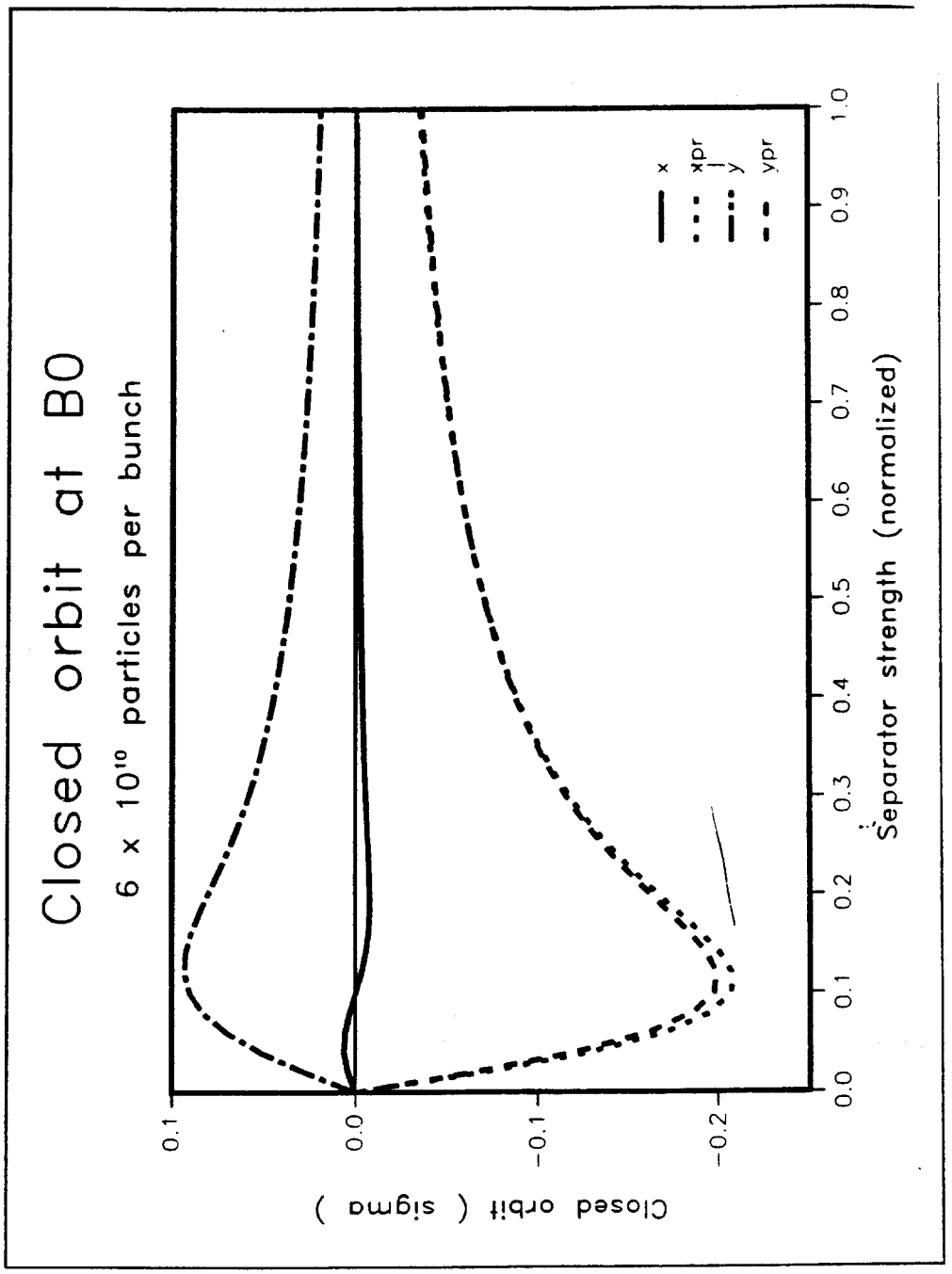
Closed orbit at B0
6 x 10¹⁰ particles per bunch
Closed orbit (sigma)
0.1
0.0
−0.1
−0.2
0.0
0.1
0.2
0.3
0.4
0.5
0.6
0.7
0.8
0.9
1.0
Separator strength (normalized)
x
xpr
y
ypr

Figure 2(a)

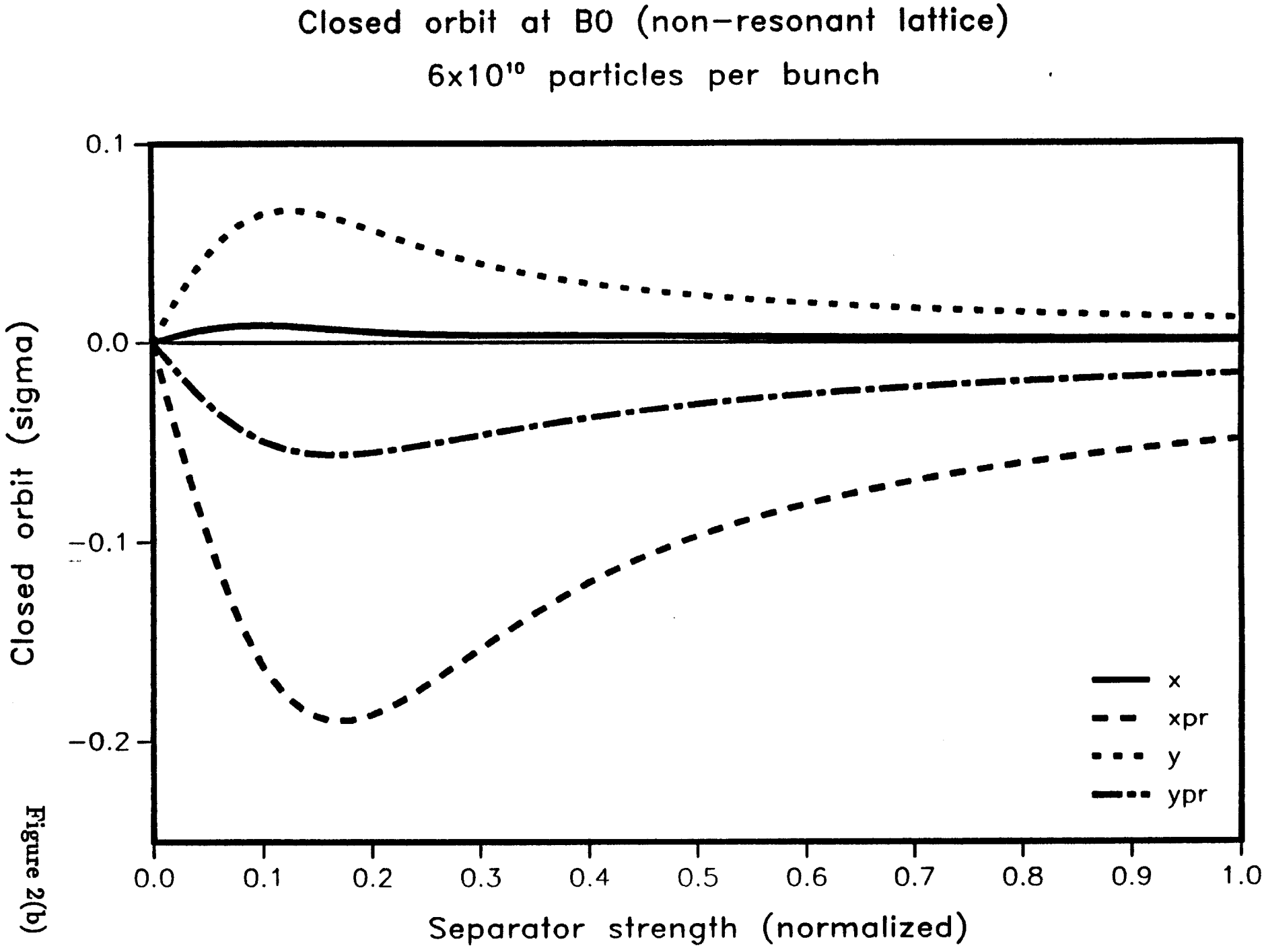
Closed orbit at B0 (non-resonant lattice)
6x10¹⁰ particles per bunch
0.1
0.0
−0.1
−0.2
Closed orbit (sigma)
0.0
0.1
0.2
0.3
0.4
0.5
0.6
0.7
0.8
0.9
1.0
Separator strength (normalized)
x
xpr
y
ypr

Figure 2(b)

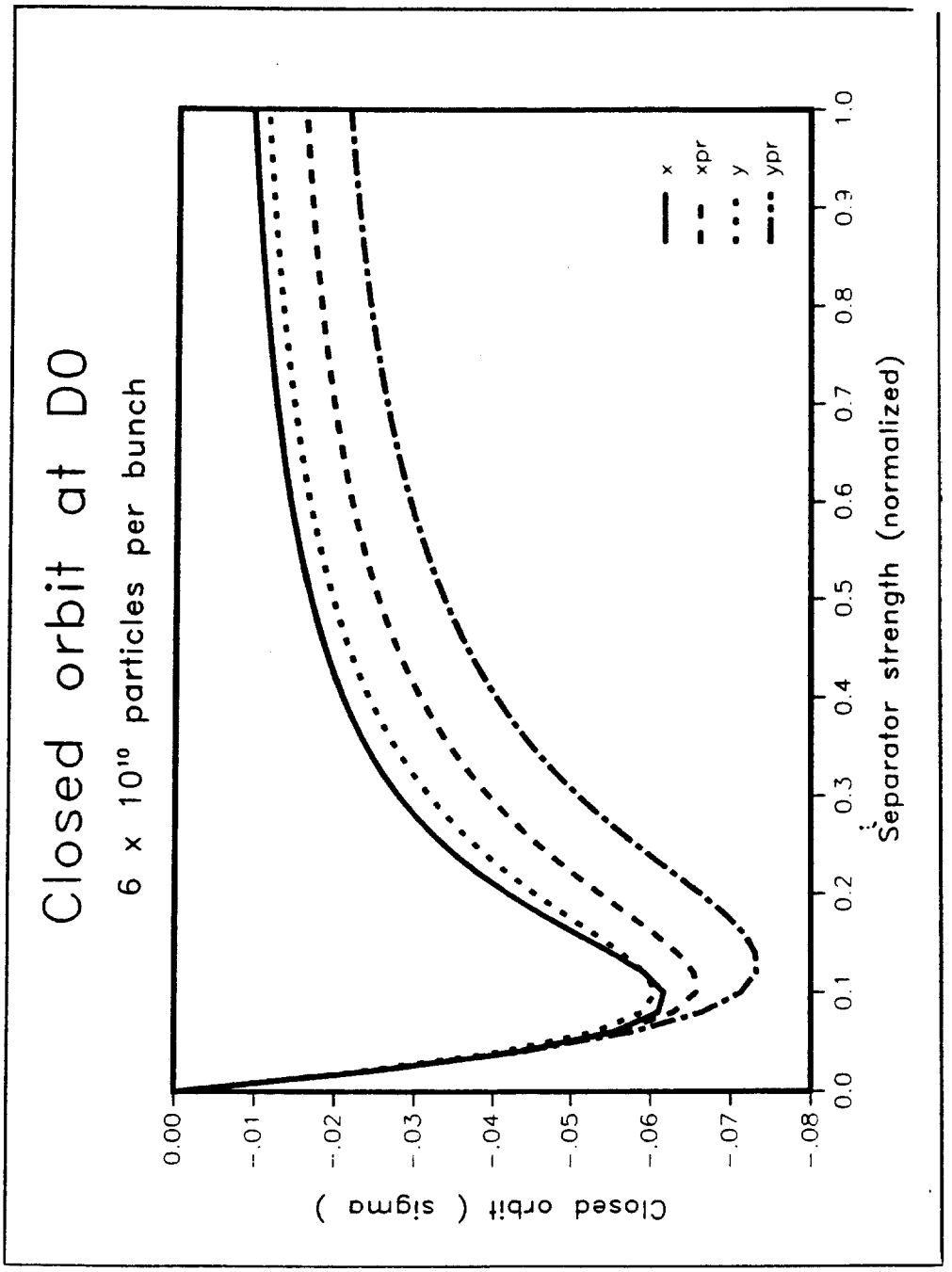
Closed orbit at D0
6 x 10¹⁰ particles per bunch
Closed orbit (sigma)
0.00
-.01
-.02
-.03
-.04
-.05
-.06
-.07
-.08
0.0
0.1
0.2
0.3
0.4
0.5
0.6
0.7
0.8
0.9
1.0
Separator strength (normalized)
x
xpr
y
ypr

Figure 3(a)

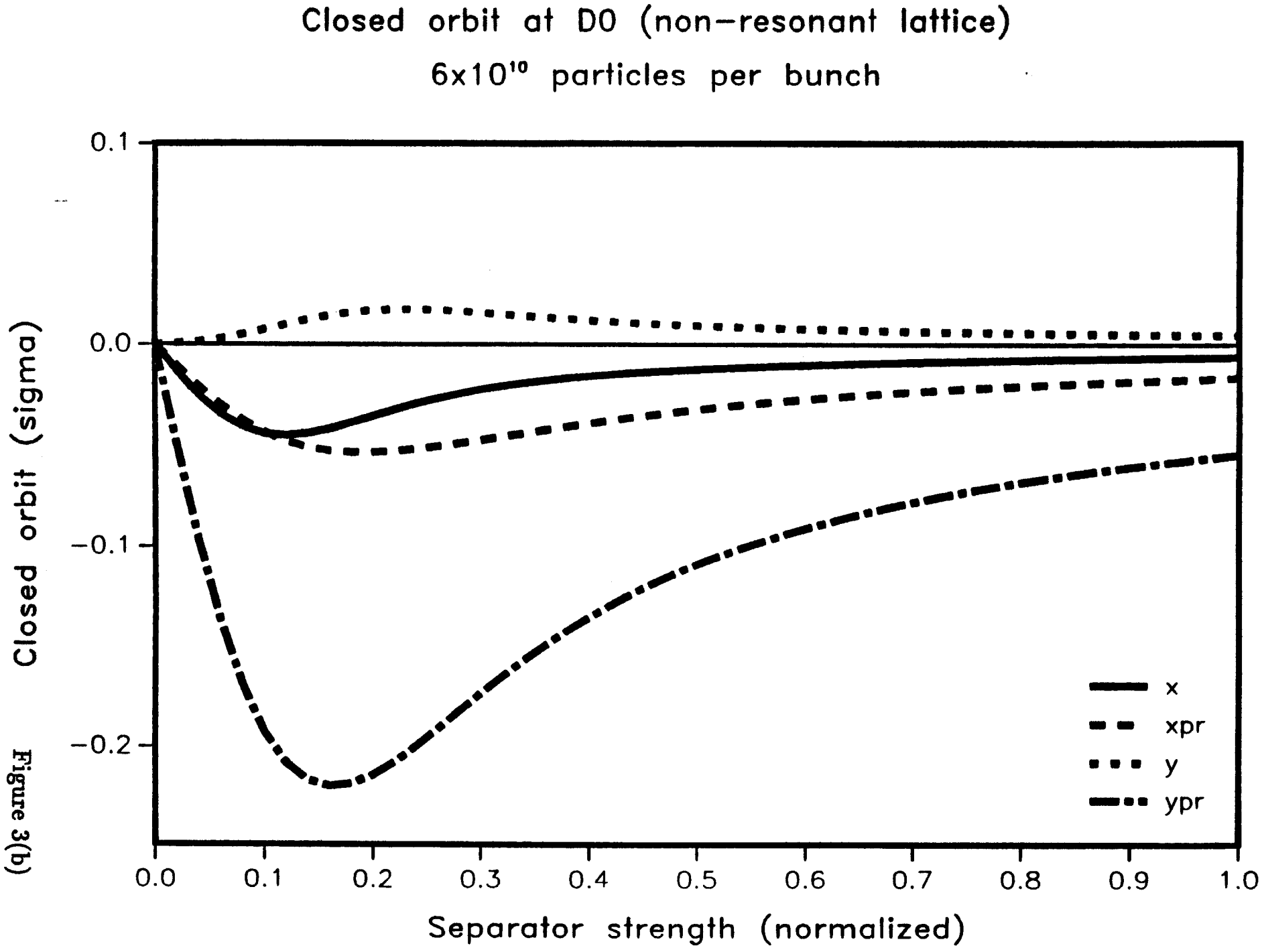
Closed orbit at D0 (non-resonant lattice)
6x10¹⁰ particles per bunch
0.1
0.0
-0.1
-0.2
Closed orbit (sigma)
0.0
0.1
0.2
0.3
0.4
0.5
0.6
0.7
0.8
0.9
1.0
Separator strength (normalized)
x
xpr
y
ypr

Figure 3(b)

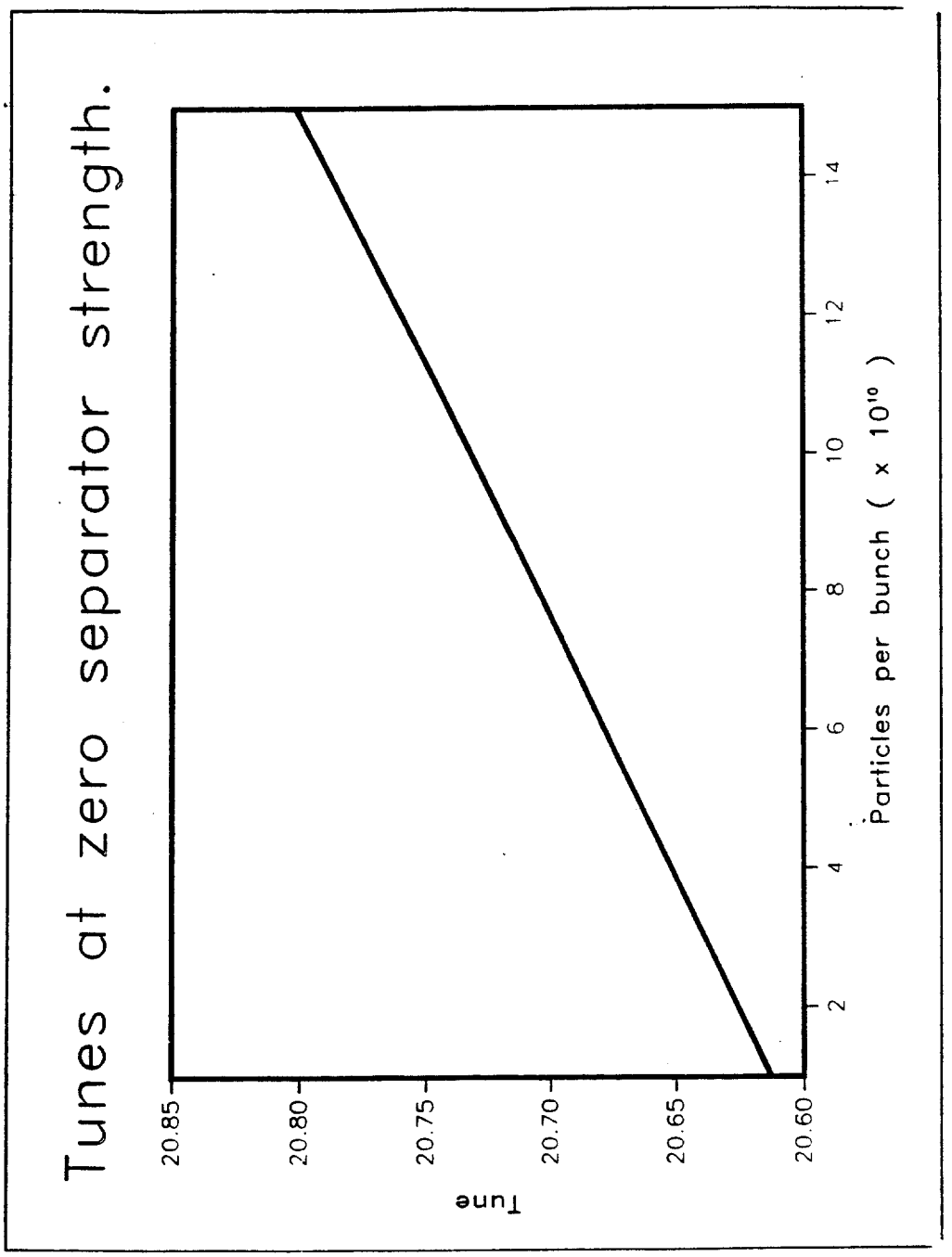
Tunes at zero separator strength.
Tune
20.85
20.80
20.75
20.70
20.65
20.60
2
4
6
8
10
12
14
Particles per bunch (x 10¹⁰)

Figure 4

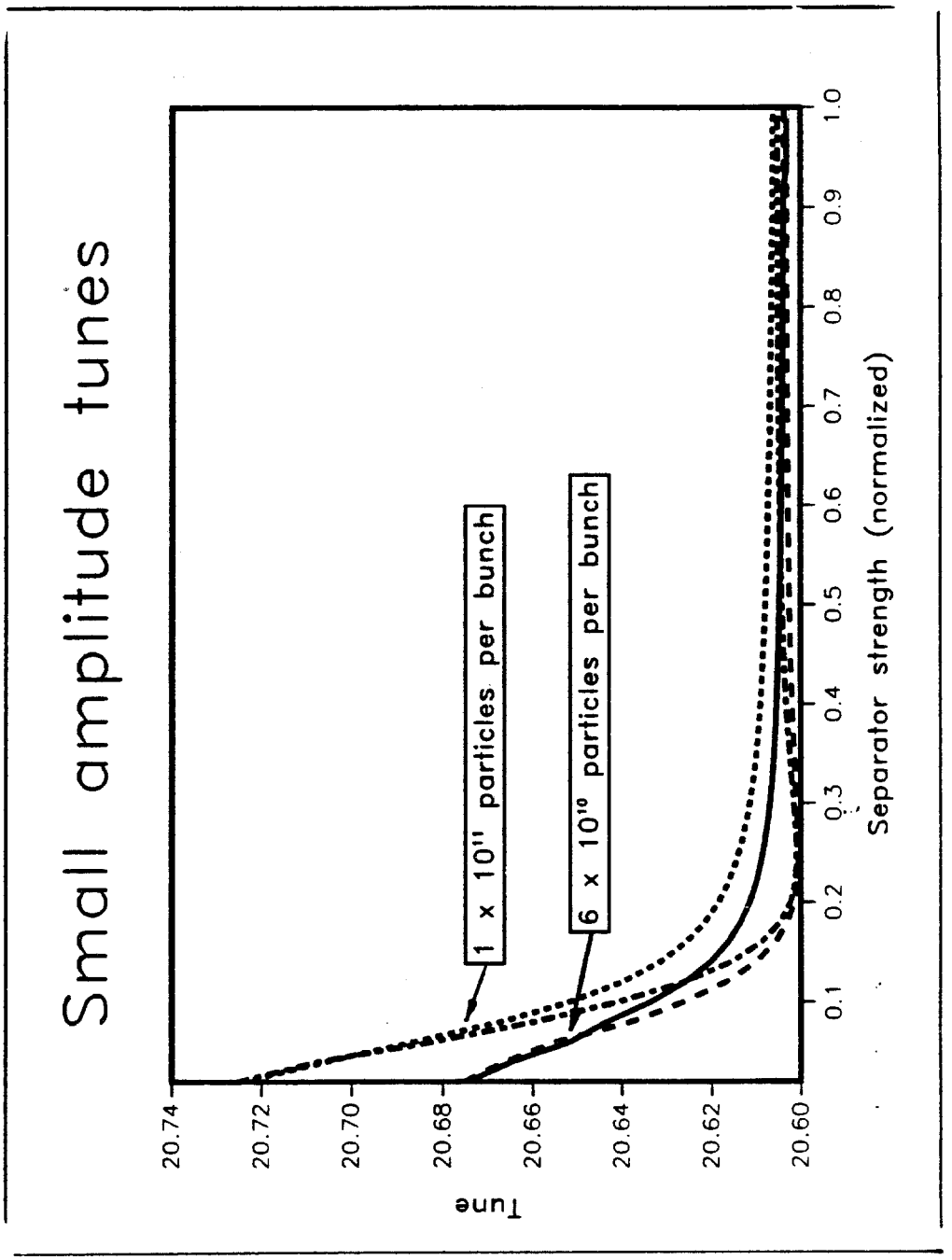
Small amplitude tunes
Tune
20.74
20.72
20.70
20.68
20.66
20.64
20.62
20.60
0.1
0.2
0.3
0.4
0.5
0.6
0.7
0.8
0.9
1.0
Separator strength (normalized)
1 x 10¹¹ particles per bunch
6 x 10¹⁰ particles per bunch

Figure 5

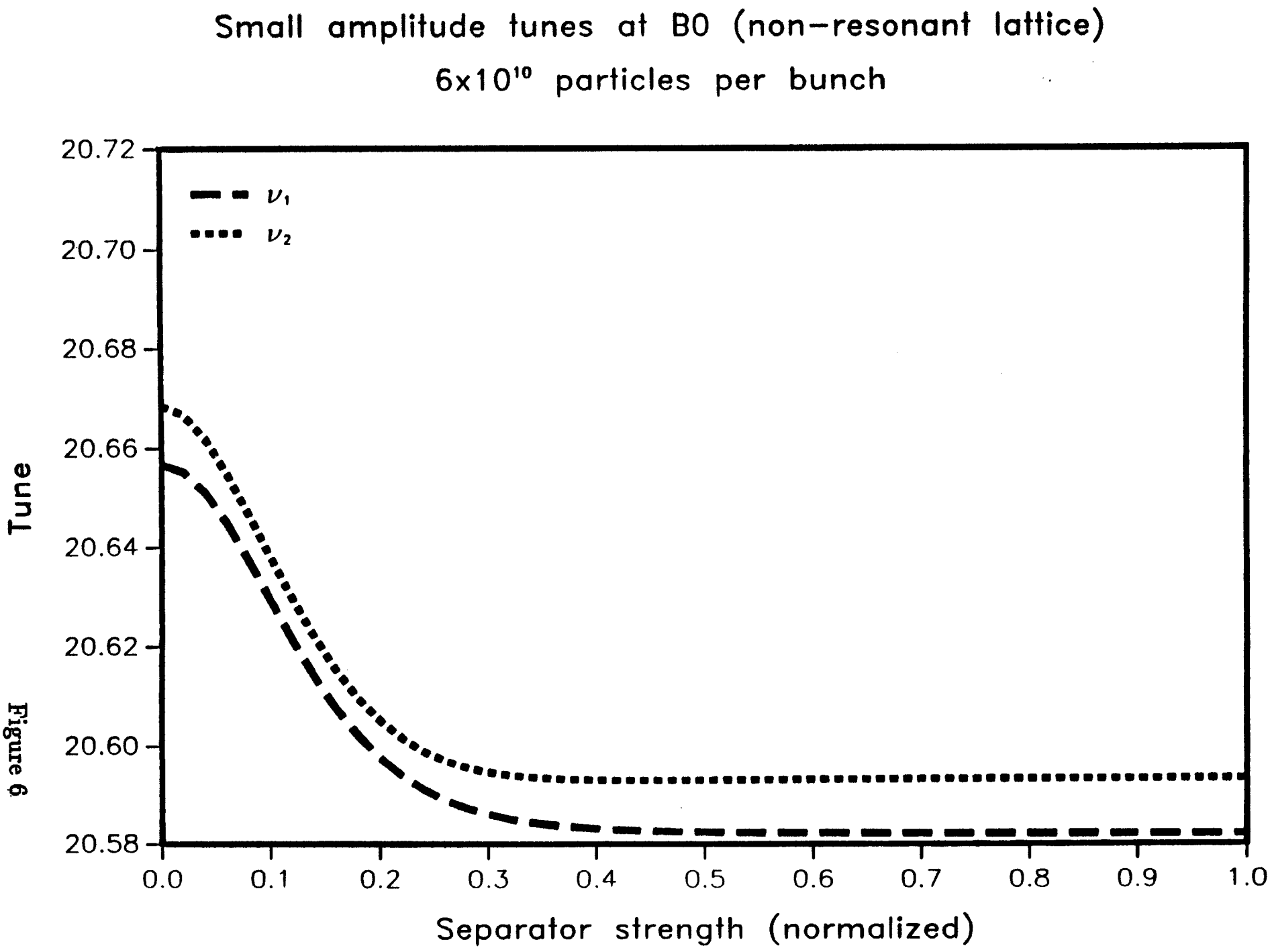
Small amplitude tunes at B0 (non-resonant lattice)
6x10¹⁰ particles per bunch
ν_1
ν_2
Tune
20.72
20.70
20.68
20.66
20.64
20.62
20.60
20.58
0.0
0.1
0.2
0.3
0.4
0.5
0.6
0.7
0.8
0.9
1.0
Separator strength (normalized)

Figure 6

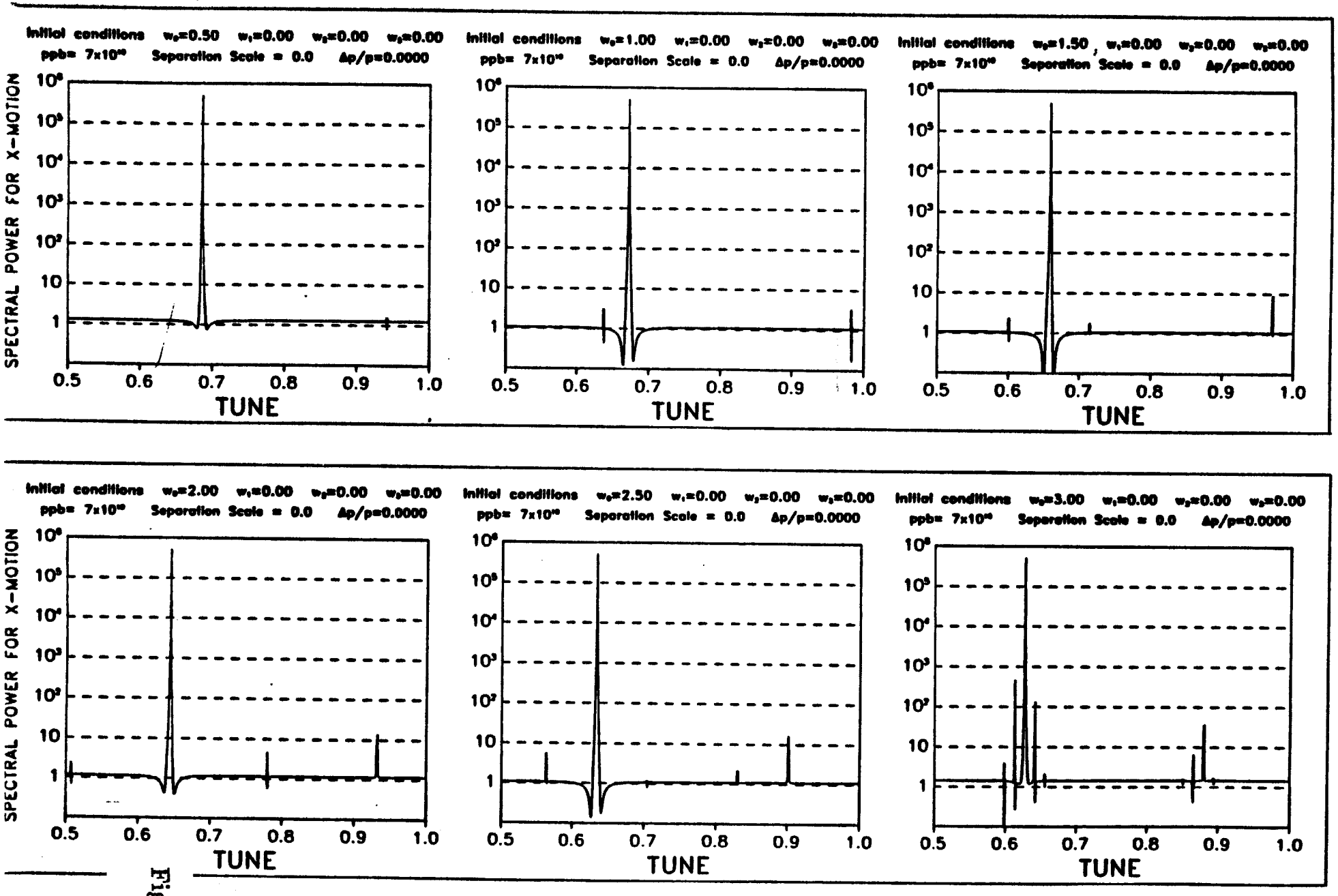
Initial conditions w_0=0.50 w_1=0.00 w_2=0.00 w_3=0.00
ppb= 7x10^{10} Separation Scale = 0.0 Δp/p=0.0000
Initial conditions w_0=1.00 w_1=0.00 w_2=0.00 w_3=0.00
ppb= 7x10^{10} Separation Scale = 0.0 Δp/p=0.0000
Initial conditions w_0=1.50 w_1=0.00 w_2=0.00 w_3=0.00
ppb= 7x10^{10} Separation Scale = 0.0 Δp/p=0.0000
Initial conditions w_0=2.00 w_1=0.00 w_2=0.00 w_3=0.00
ppb= 7x10^{10} Separation Scale = 0.0 Δp/p=0.0000
Initial conditions w_0=2.50 w_1=0.00 w_2=0.00 w_3=0.00
ppb= 7x10^{10} Separation Scale = 0.0 Δp/p=0.0000
Initial conditions w_0=3.00 w_1=0.00 w_2=0.00 w_3=0.00
ppb= 7x10^{10} Separation Scale = 0.0 Δp/p=0.0000
SPECTRAL POWER FOR X-MOTION
10^6
10^5
10^4
10^3
10^2
10
1
0.5 0.6 0.7 0.8 0.9 1.0
TUNE

Figure 7

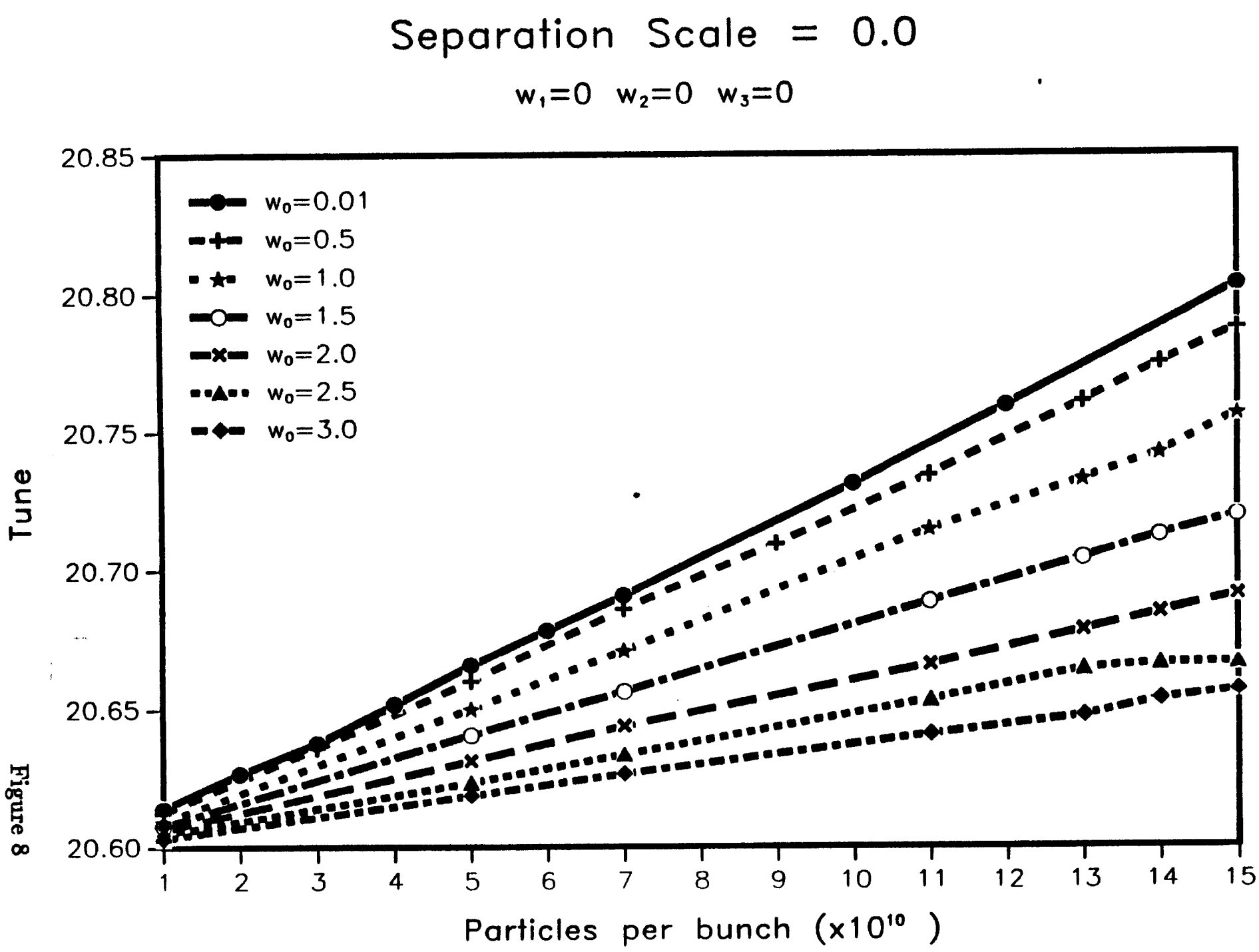
Separation Scale = 0.0
w1=0 w2=0 w3=0
w0=0.01
w0=0.5
w0=1.0
w0=1.5
w0=2.0
w0=2.5
w0=3.0
Tune
20.85
20.80
20.75
20.70
20.65
20.60
1
2
3
4
5
6
7
8
9
10
11
12
13
14
15
Particles per bunch (x10^10)

Figure 8

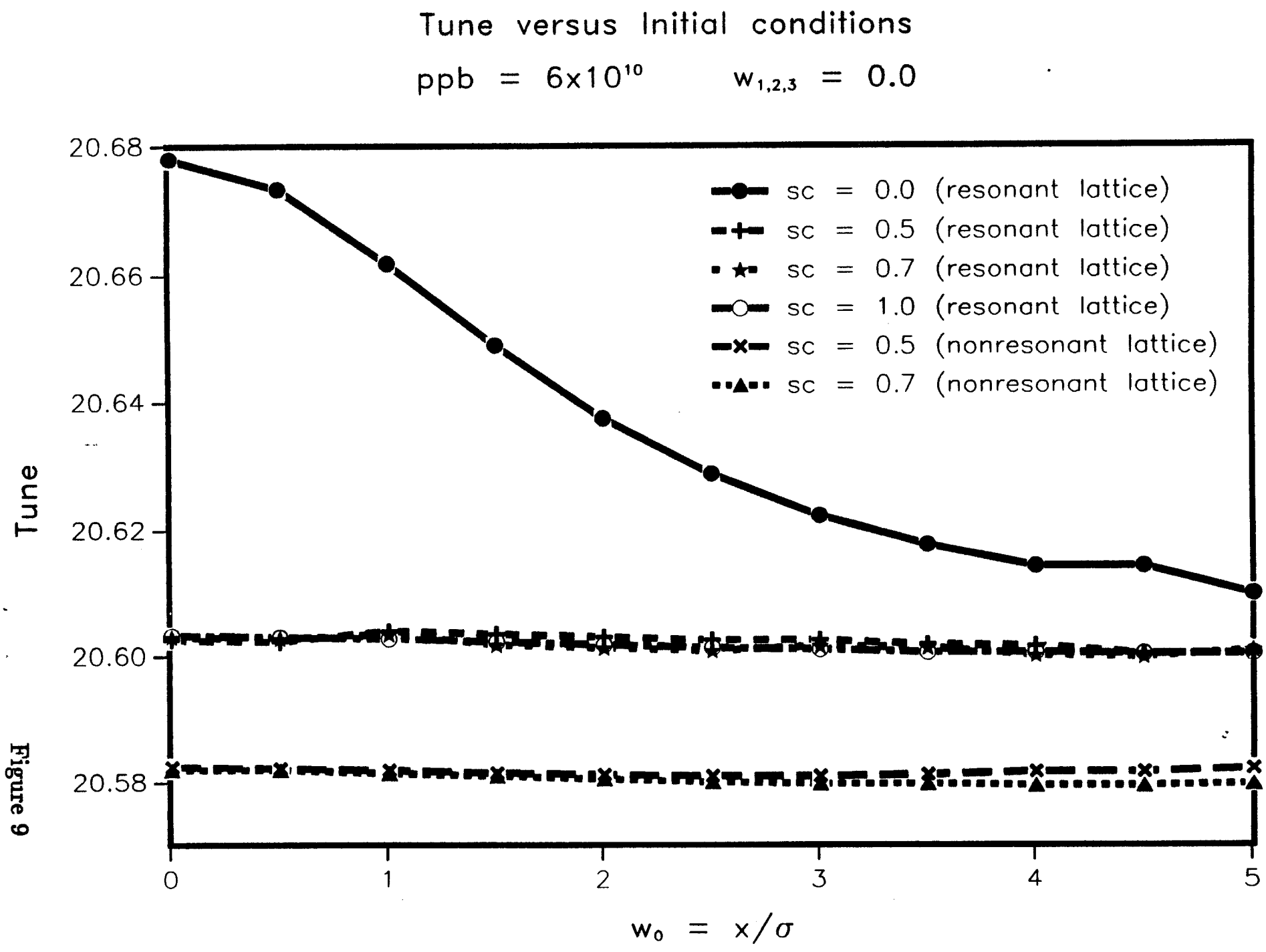
Tune versus Initial conditions
ppb = 6x10^10 w1,2,3 = 0.0
sc = 0.0 (resonant lattice)
sc = 0.5 (resonant lattice)
sc = 0.7 (resonant lattice)
sc = 1.0 (resonant lattice)
sc = 0.5 (nonresonant lattice)
sc = 0.7 (nonresonant lattice)
Tune
20.68
20.66
20.64
20.62
20.60
20.58
0
1
2
3
4
5
w0 = x/σ

Figure 9

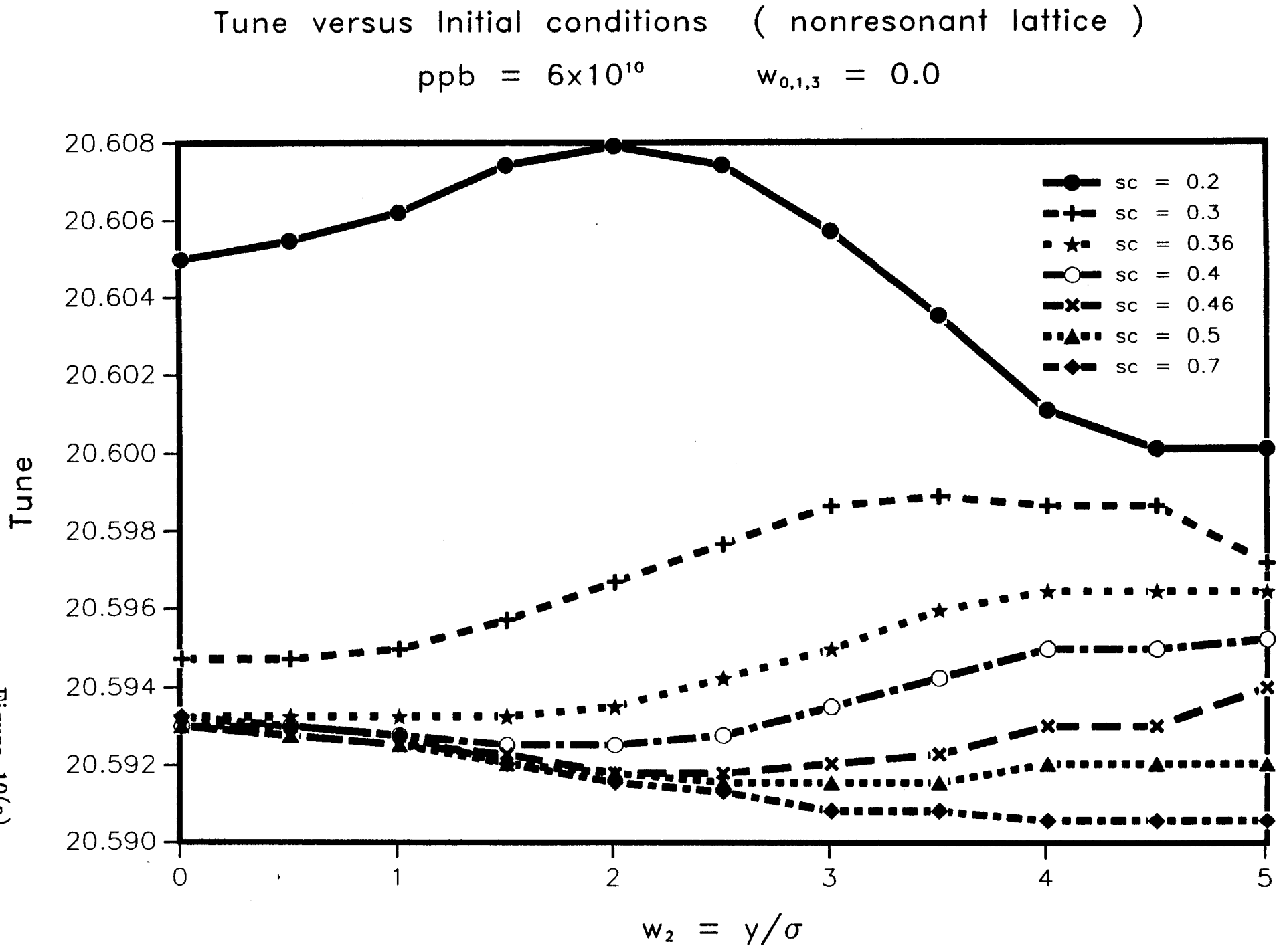
Tune versus Initial conditions (nonresonant lattice)
ppb = 6x10^10 w0,1,3 = 0.0
Tune
20.608
20.606
20.604
20.602
20.600
20.598
20.596
20.594
20.592
20.590
0
1
2
3
4
5
w2 = y/σ
sc = 0.2
sc = 0.3
sc = 0.36
sc = 0.4
sc = 0.46
sc = 0.5
sc = 0.7

Figure 10(a)

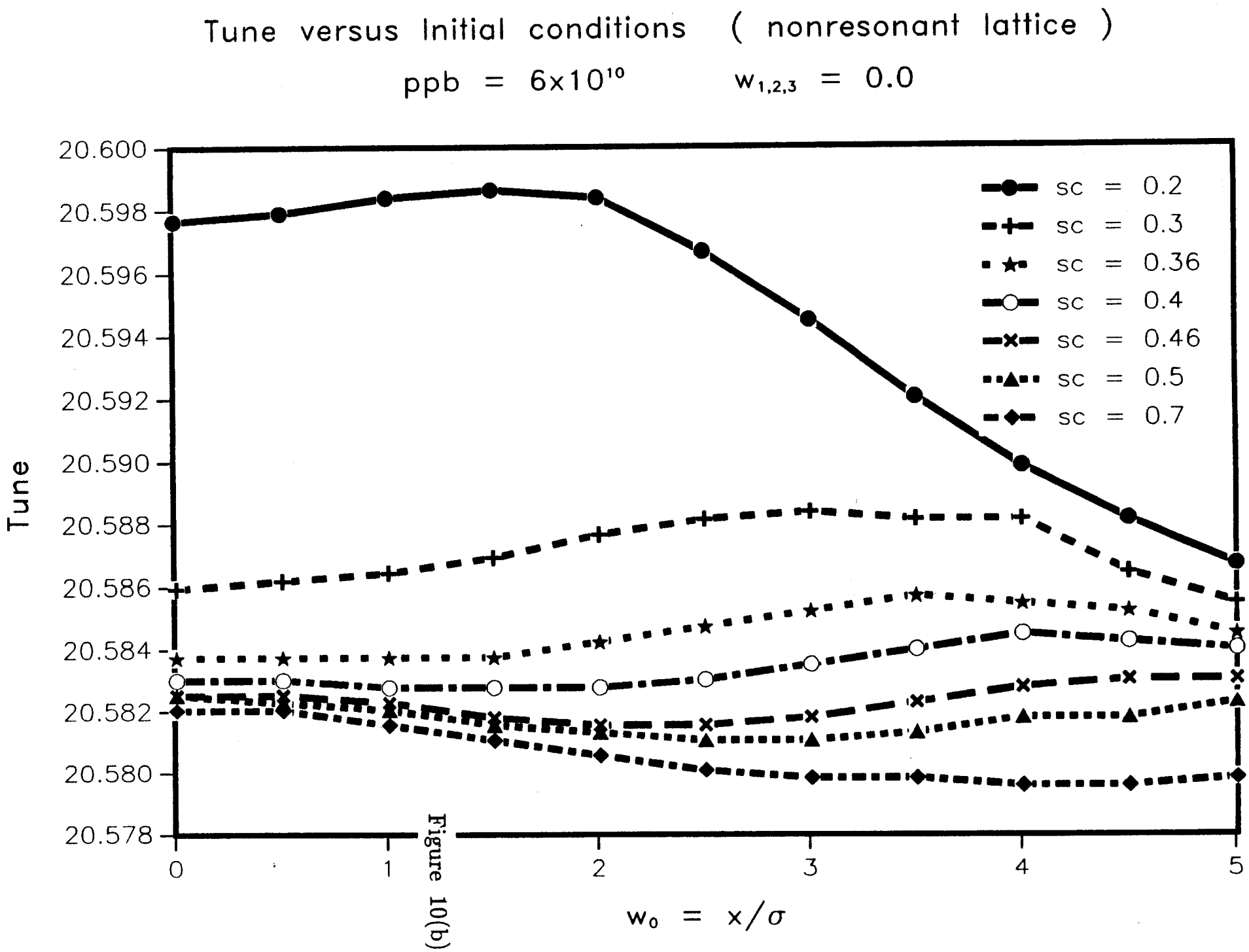
Tune versus Initial conditions (nonresonant lattice)
ppb = 6x10¹⁰ w1,2,3 = 0.0
Tune
20.600
20.598
20.596
20.594
20.592
20.590
20.588
20.586
20.584
20.582
20.580
20.578
0
1
2
3
4
5
w0 = x/σ
sc = 0.2
sc = 0.3
sc = 0.36
sc = 0.4
sc = 0.46
sc = 0.5
sc = 0.7

Figure 10(b)

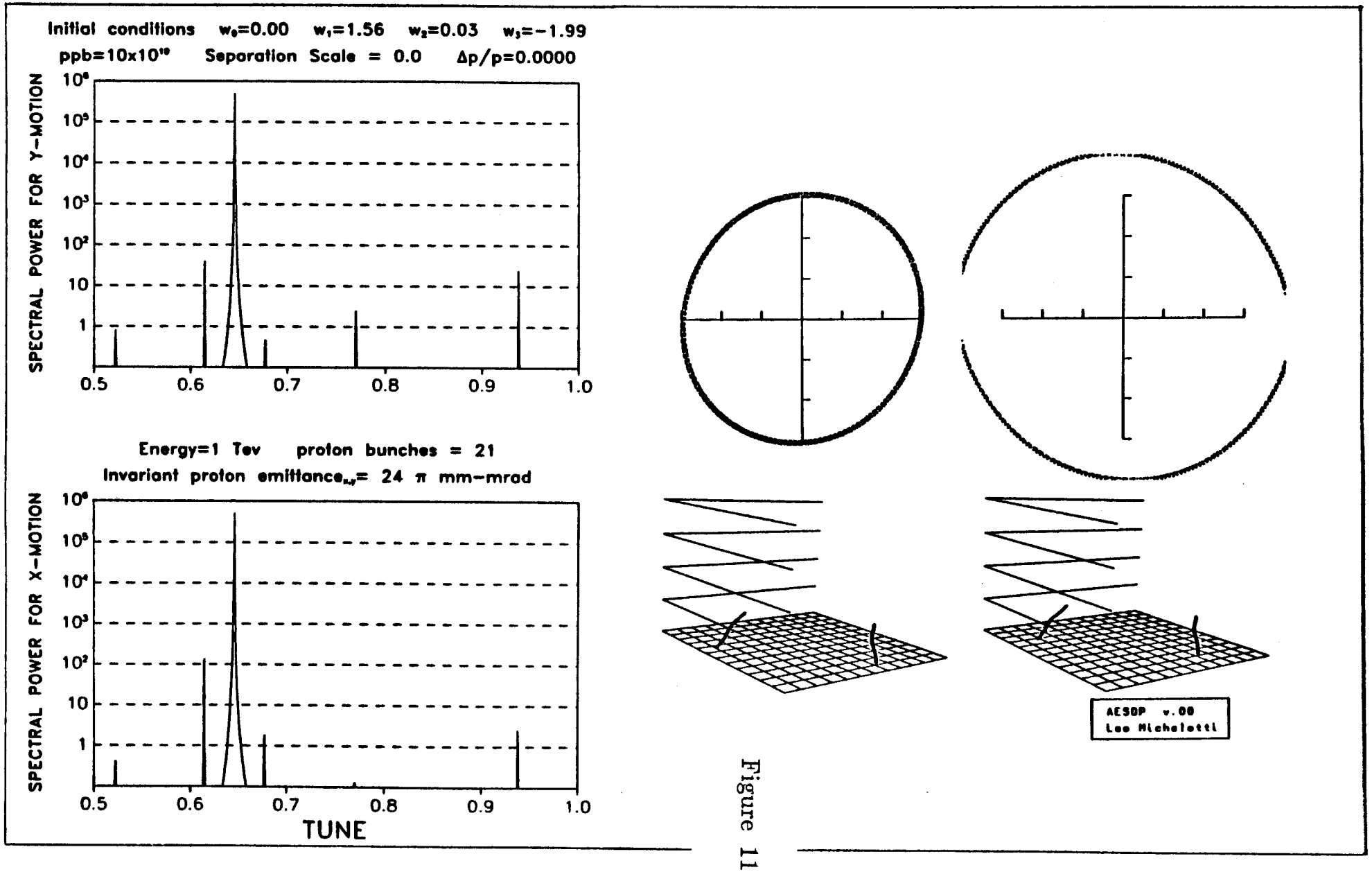
Initial conditions w_0=0.00 w_1=1.56 w_2=0.03 w_3=-1.99
ppb=10x10^{10} Separation Scale = 0.0 Δp/p=0.0000
SPECTRAL POWER FOR Y-MOTION
Energy=1 Tev proton bunches = 21
Invariant proton emittance$_{x,y}$= 24 π mm-mrad
SPECTRAL POWER FOR X-MOTION
TUNE
AESOP v.00
Leo Michelotti

Figure 11(a)

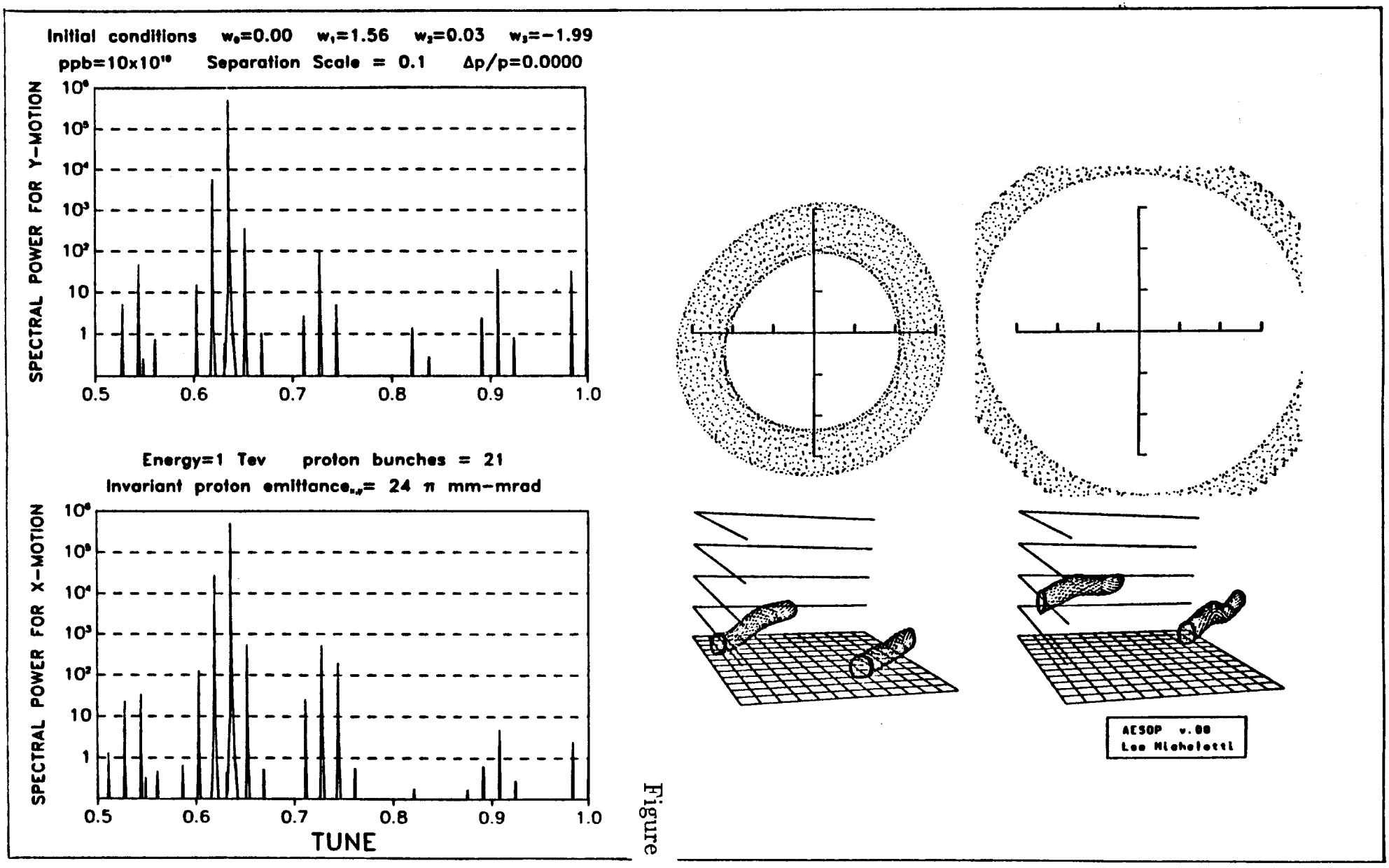
Initial conditions w_0=0.00 w_1=1.56 w_2=0.03 w_3=−1.99
ppb=10x10¹⁰ Separation Scale = 0.1 Δp/p=0.0000
SPECTRAL POWER FOR Y-MOTION
Energy=1 Tev proton bunches = 21
Invariant proton emittance$_{x,y}$= 24 π mm−mrad
SPECTRAL POWER FOR X-MOTION
TUNE
AESOP v.00
Leo Michelotti

Figure 11(b)

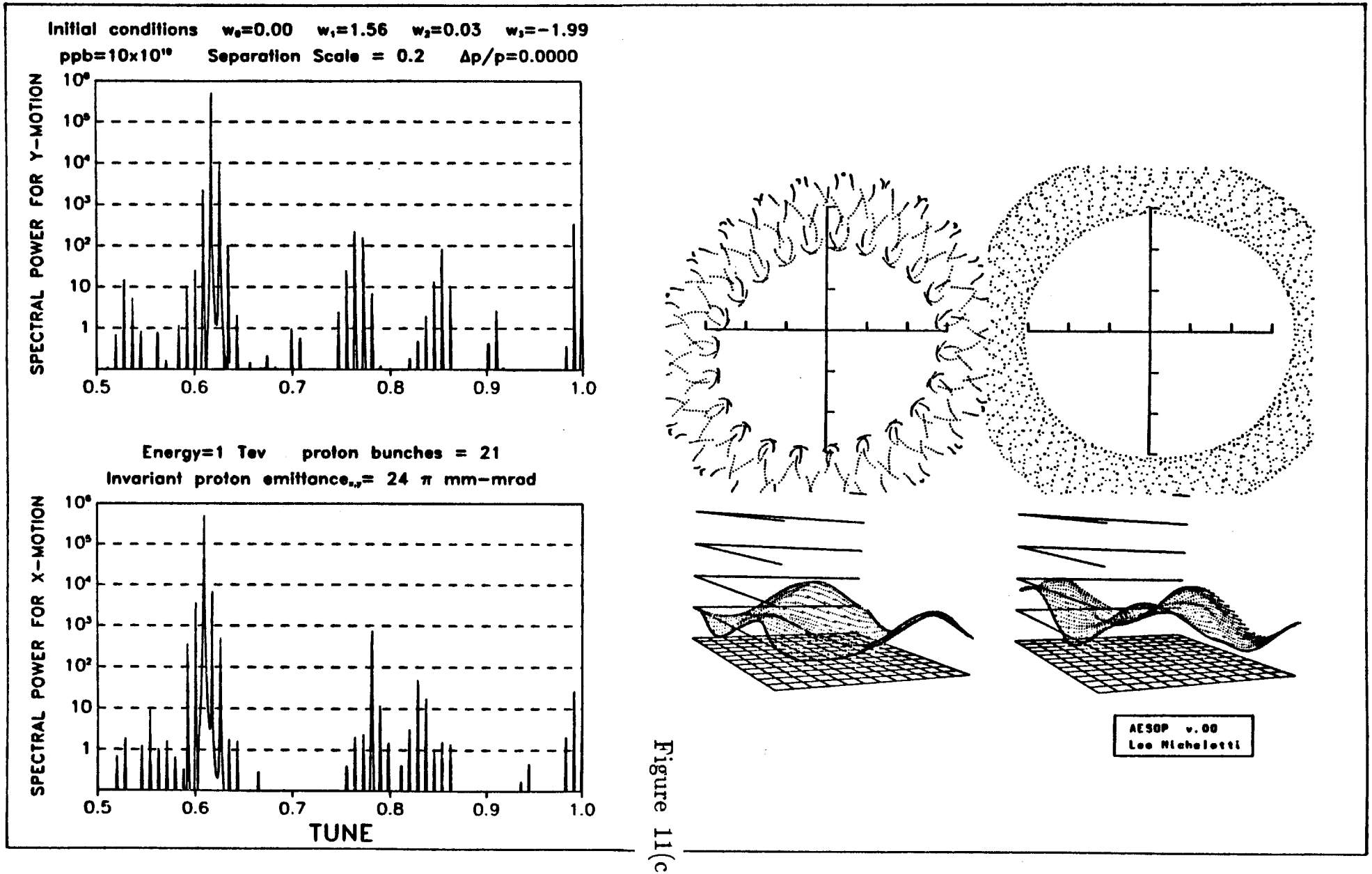
Initial conditions w_0=0.00 w_1=1.56 w_2=0.03 w_3=−1.99
ppb=10x10¹⁰ Separation Scale = 0.2 Δp/p=0.0000
SPECTRAL POWER FOR Y-MOTION
Energy=1 Tev proton bunches = 21
Invariant proton emittance$_{x,y}$= 24 π mm−mrad
SPECTRAL POWER FOR X-MOTION
TUNE
AESOP v.00
Leo Michelotti

Figure 11(c)

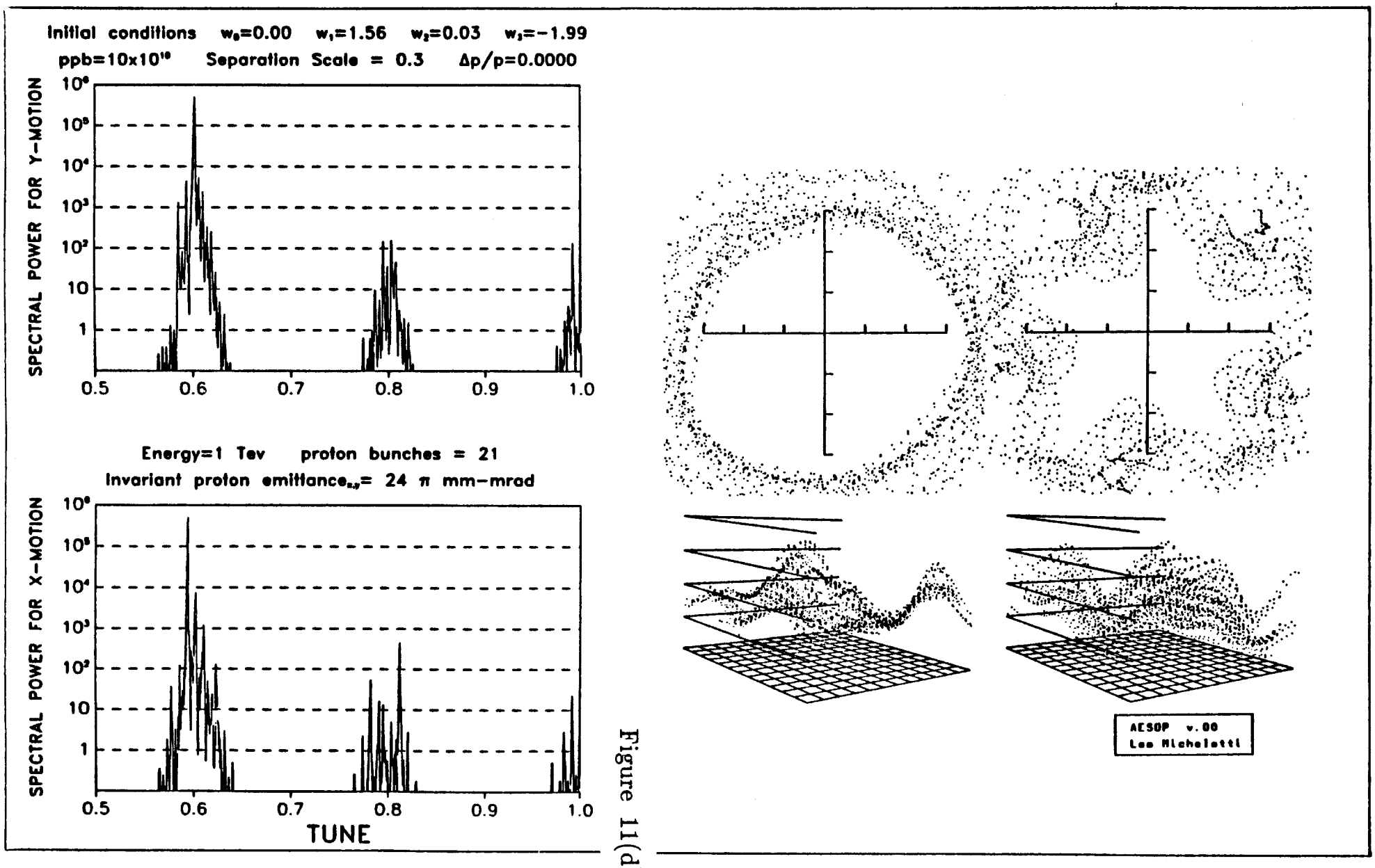
Initial conditions w_0=0.00 w_1=1.56 w_2=0.03 w_3=−1.99
ppb=10x10¹⁰ Separation Scale = 0.3 Δp/p=0.0000
SPECTRAL POWER FOR Y-MOTION
Energy=1 Tev proton bunches = 21
Invariant proton emittance$_{x,y}$= 24 π mm−mrad
SPECTRAL POWER FOR X-MOTION
TUNE
AESOP v.00
Leo Michelotti

Figure 11(d)

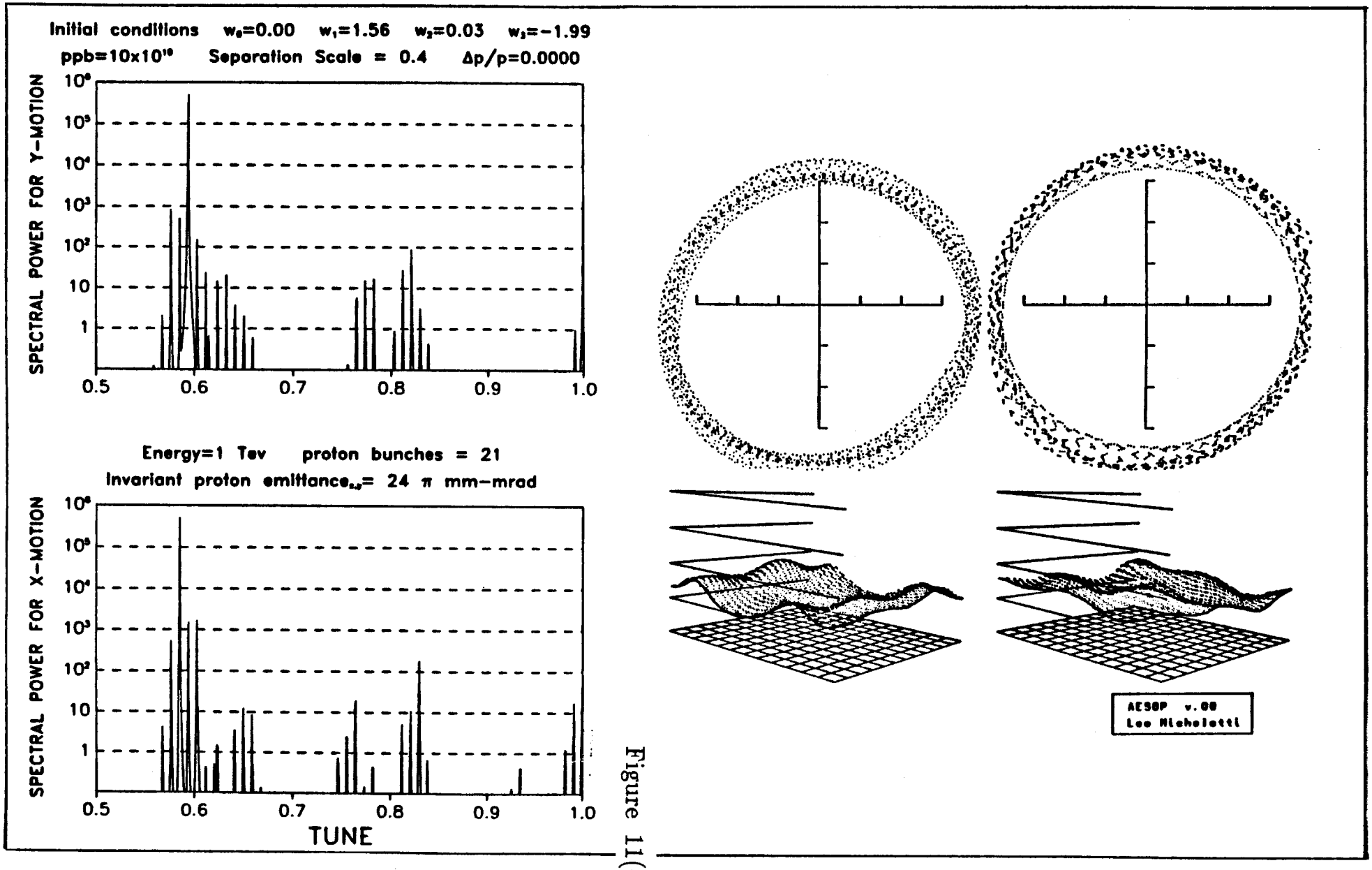
Initial conditions w_0=0.00 w_1=1.56 w_2=0.03 w_3=−1.99
ppb=10x10¹⁰ Separation Scale = 0.4 Δp/p=0.0000
SPECTRAL POWER FOR Y-MOTION
Energy=1 Tev proton bunches = 21
Invariant proton emittance$_{x,y}$= 24 π mm−mrad
SPECTRAL POWER FOR X-MOTION
TUNE
AESOP v.00
Leo Michelotti

Figure 11(e)

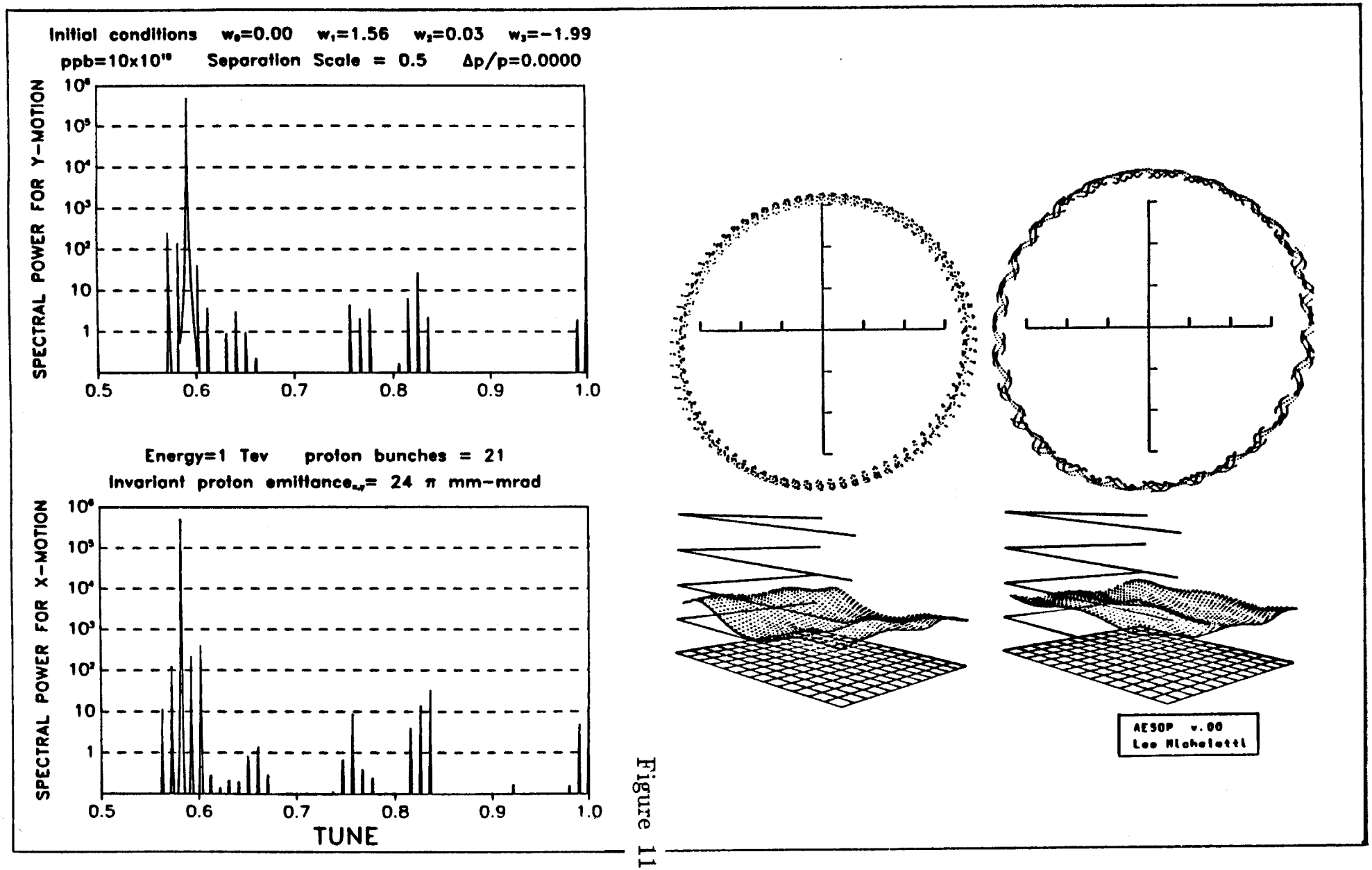
Initial conditions w_0=0.00 w_1=1.56 w_2=0.03 w_3=-1.99
ppb=10x10^{10} Separation Scale = 0.5 Δp/p=0.0000
SPECTRAL POWER FOR Y-MOTION
Energy=1 Tev proton bunches = 21
Invariant proton emittance$_{x,y}$= 24 π mm-mrad
SPECTRAL POWER FOR X-MOTION
TUNE
AESOP v.00
Lee Michelotti

Figure 11(f)

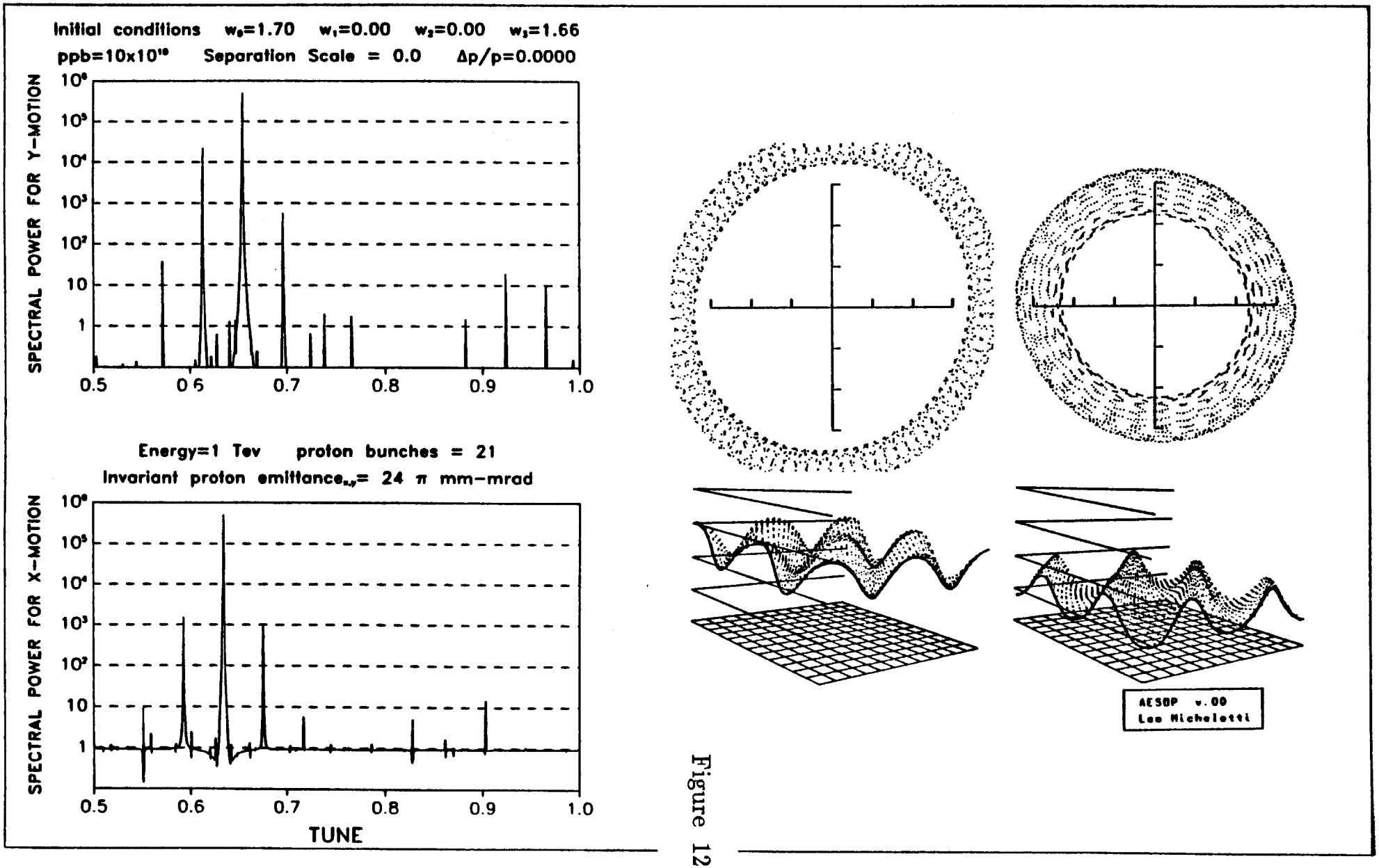
Initial conditions w_0=1.70 w_1=0.00 w_2=0.00 w_3=1.66
ppb=10x10^{10} Separation Scale = 0.0 Δp/p=0.0000
SPECTRAL POWER FOR Y-MOTION
Energy=1 Tev proton bunches = 21
Invariant proton emittance$_{x,y}$= 24 π mm-mrad
SPECTRAL POWER FOR X-MOTION
TUNE
AESOP v.00
Lee Michelotti

Figure 12(a)

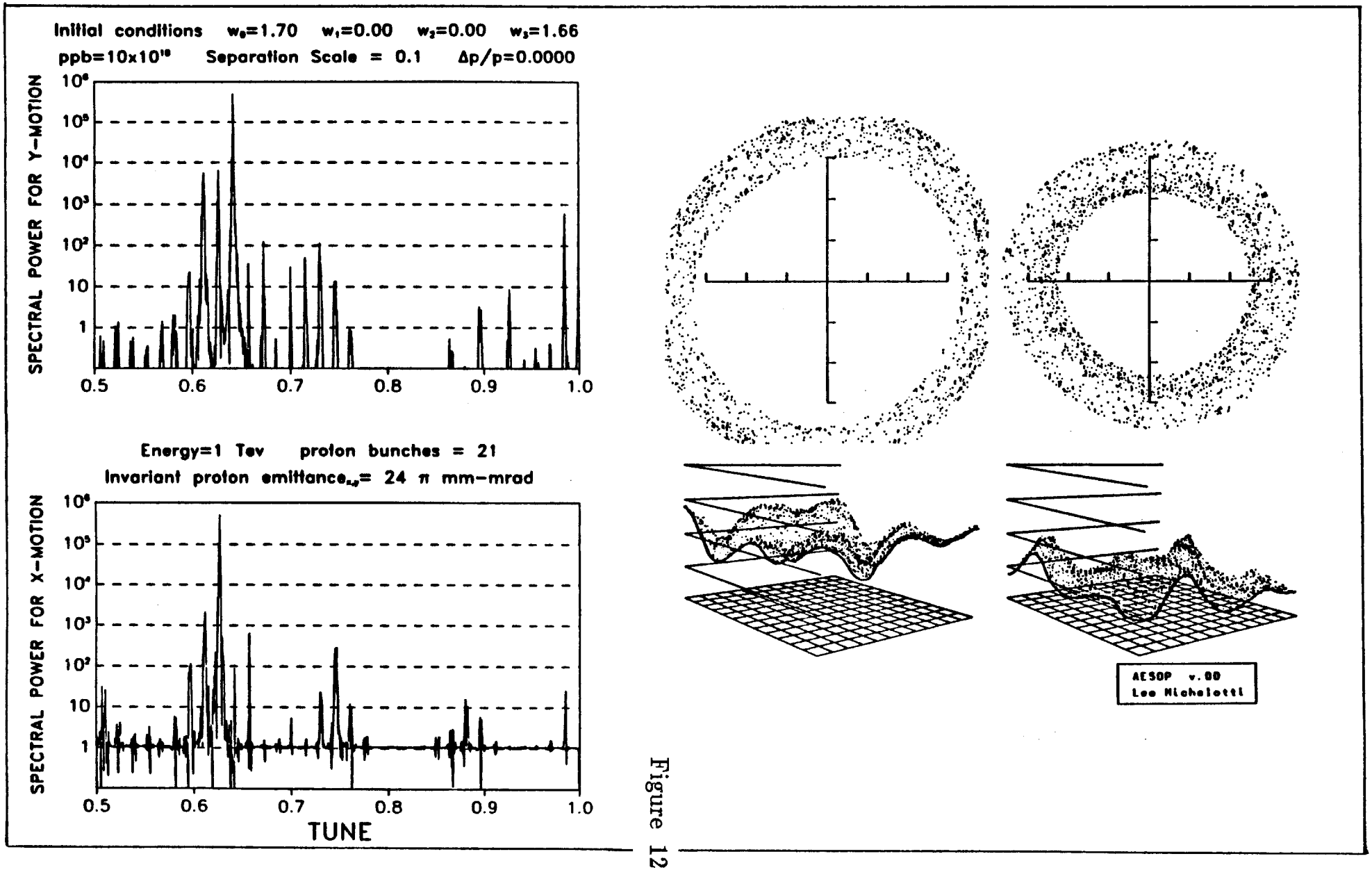
Initial conditions w_0=1.70 w_1=0.00 w_2=0.00 w_3=1.66
ppb=10x10^{10} Separation Scale = 0.1 Δp/p=0.0000
SPECTRAL POWER FOR Y-MOTION
Energy=1 Tev proton bunches = 21
Invariant proton emittance$_{x,y}$= 24 π mm-mrad
SPECTRAL POWER FOR X-MOTION
TUNE
AESOP v.00
Lee Michelotti

Figure 12(b)

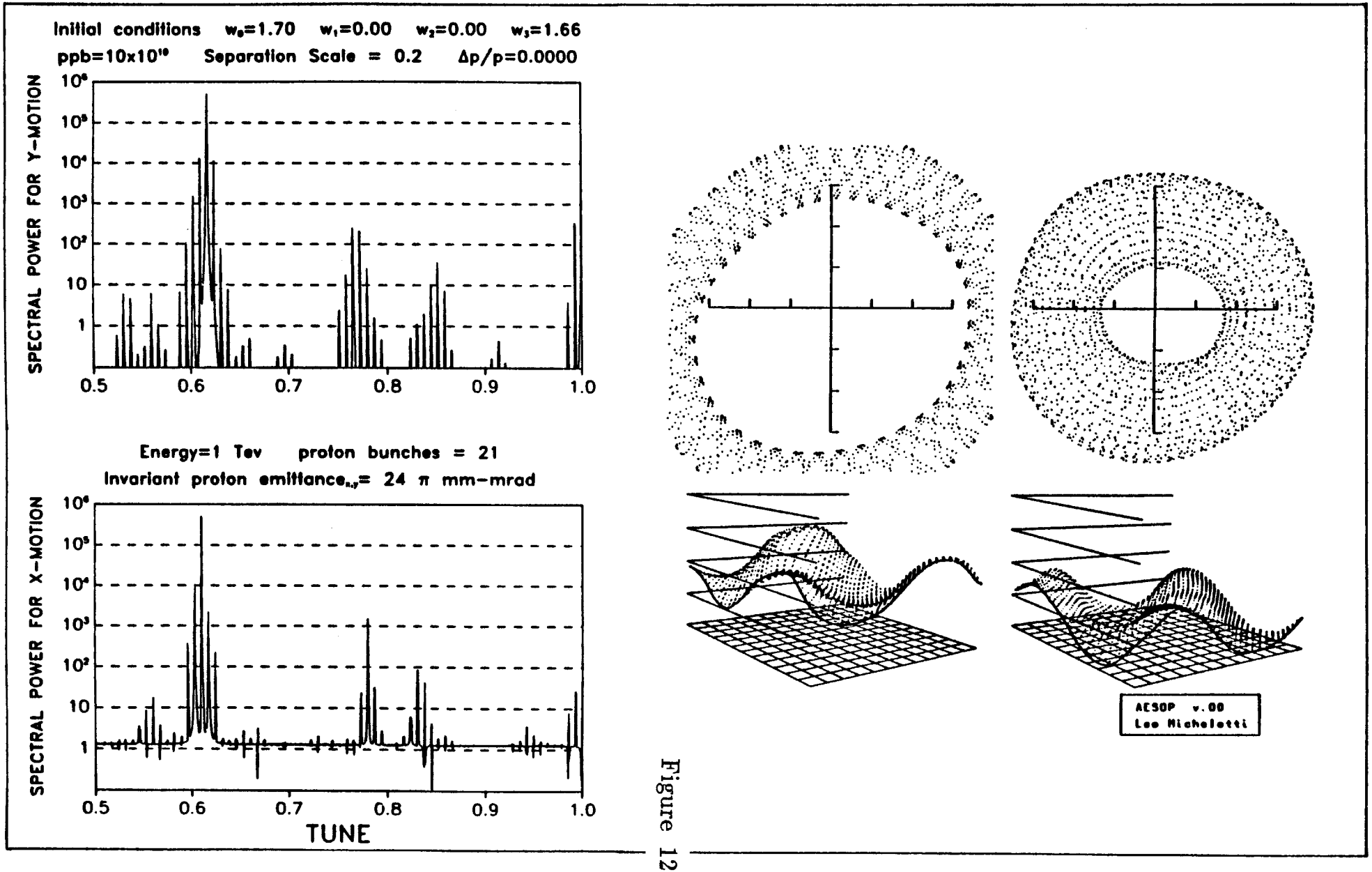
Initial conditions w_0=1.70 w_1=0.00 w_2=0.00 w_3=1.66
ppb=10x10^{10} Separation Scale = 0.2 Δp/p=0.0000
SPECTRAL POWER FOR Y-MOTION
Energy=1 Tev proton bunches = 21
Invariant proton emittance$_{x,y}$= 24 π mm-mrad
SPECTRAL POWER FOR X-MOTION
TUNE
AESOP v.00
Leo Michelotti

Figure 12(c)

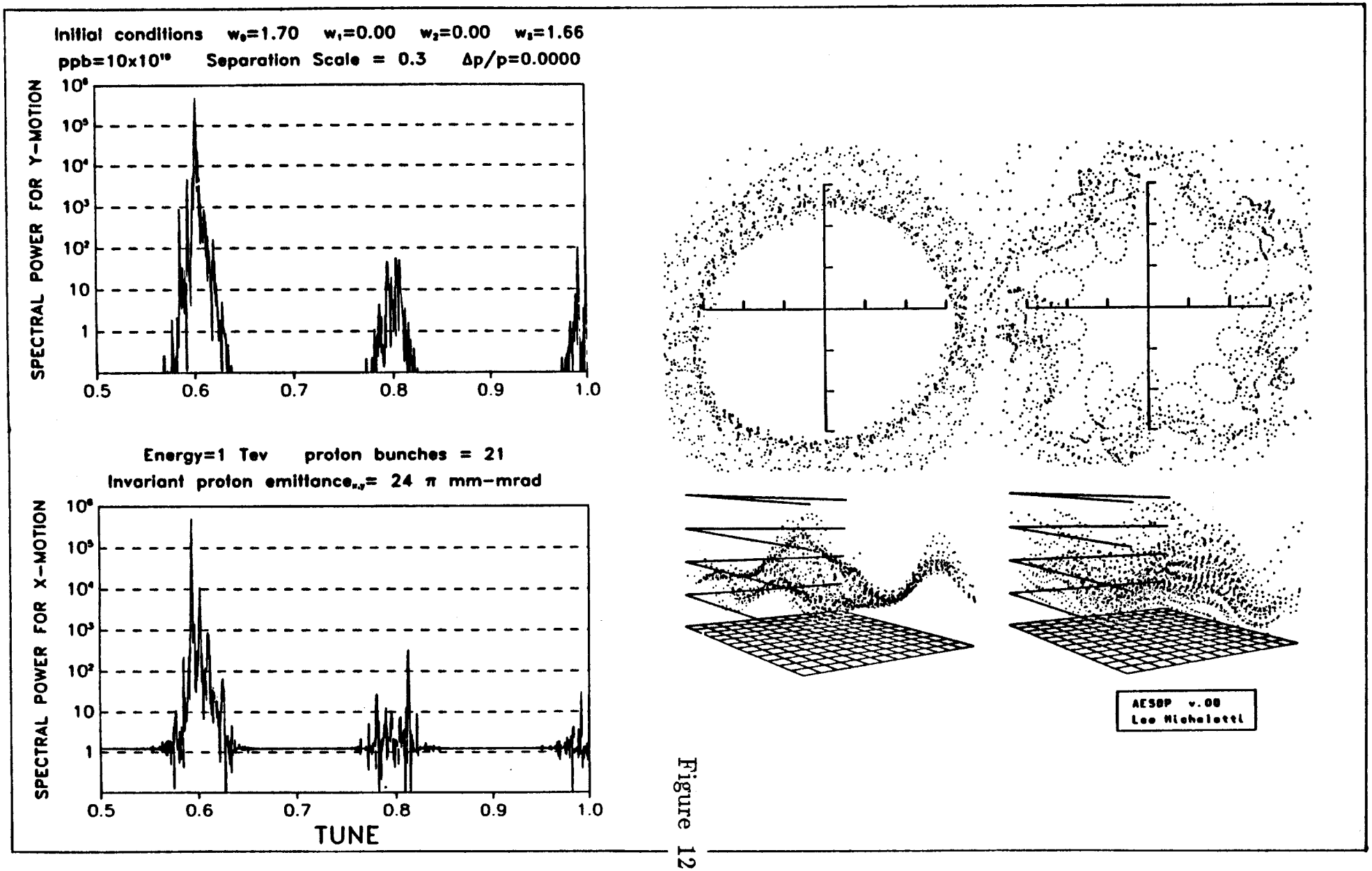
Initial conditions w_0=1.70 w_1=0.00 w_2=0.00 w_3=1.66
ppb=10x10^{10} Separation Scale = 0.3 Δp/p=0.0000
SPECTRAL POWER FOR Y-MOTION
Energy=1 Tev proton bunches = 21
Invariant proton emittance$_{x,y}$= 24 π mm-mrad
SPECTRAL POWER FOR X-MOTION
TUNE
AESOP v.00
Leo Michelotti

Figure 12(d)

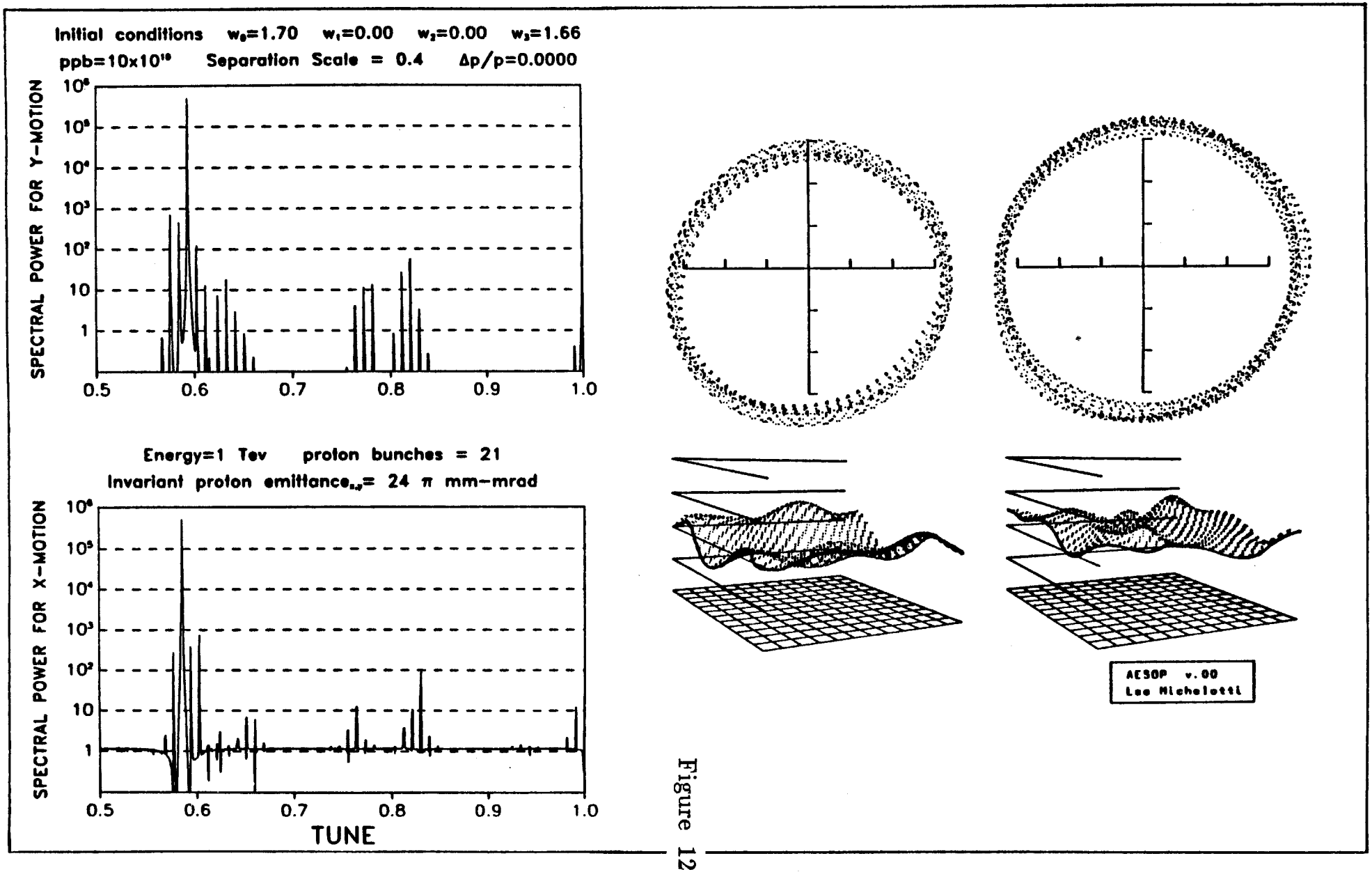
Initial conditions w_0=1.70 w_1=0.00 w_2=0.00 w_3=1.66
ppb=10x10^{10} Separation Scale = 0.4 Δp/p=0.0000
SPECTRAL POWER FOR Y-MOTION
Energy=1 Tev proton bunches = 21
Invariant proton emittance$_{x,y}$= 24 π mm-mrad
SPECTRAL POWER FOR X-MOTION
TUNE
AESOP v.00
Lee Michelotti

Figure 12(e)

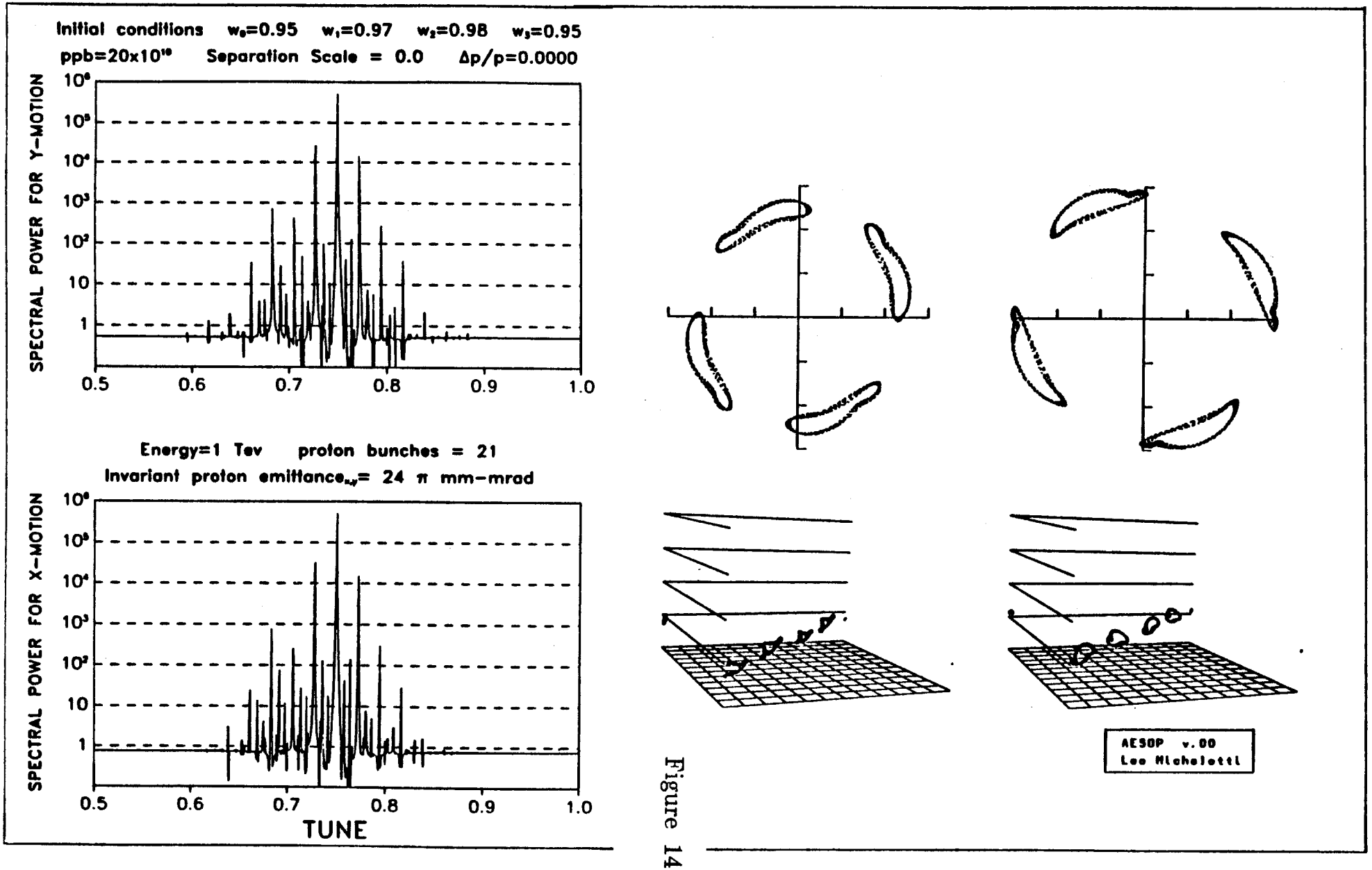
Initial conditions w_0=0.95 w_1=0.97 w_2=0.98 w_3=0.95
ppb=20x10¹⁰ Separation Scale = 0.0 Δp/p=0.0000
SPECTRAL POWER FOR Y-MOTION
Energy=1 Tev proton bunches = 21
Invariant proton emittance$_{x,y}$= 24 π mm-mrad
SPECTRAL POWER FOR X-MOTION
TUNE
AESOP v.00
Leo Michelotti

Figure 14(a)

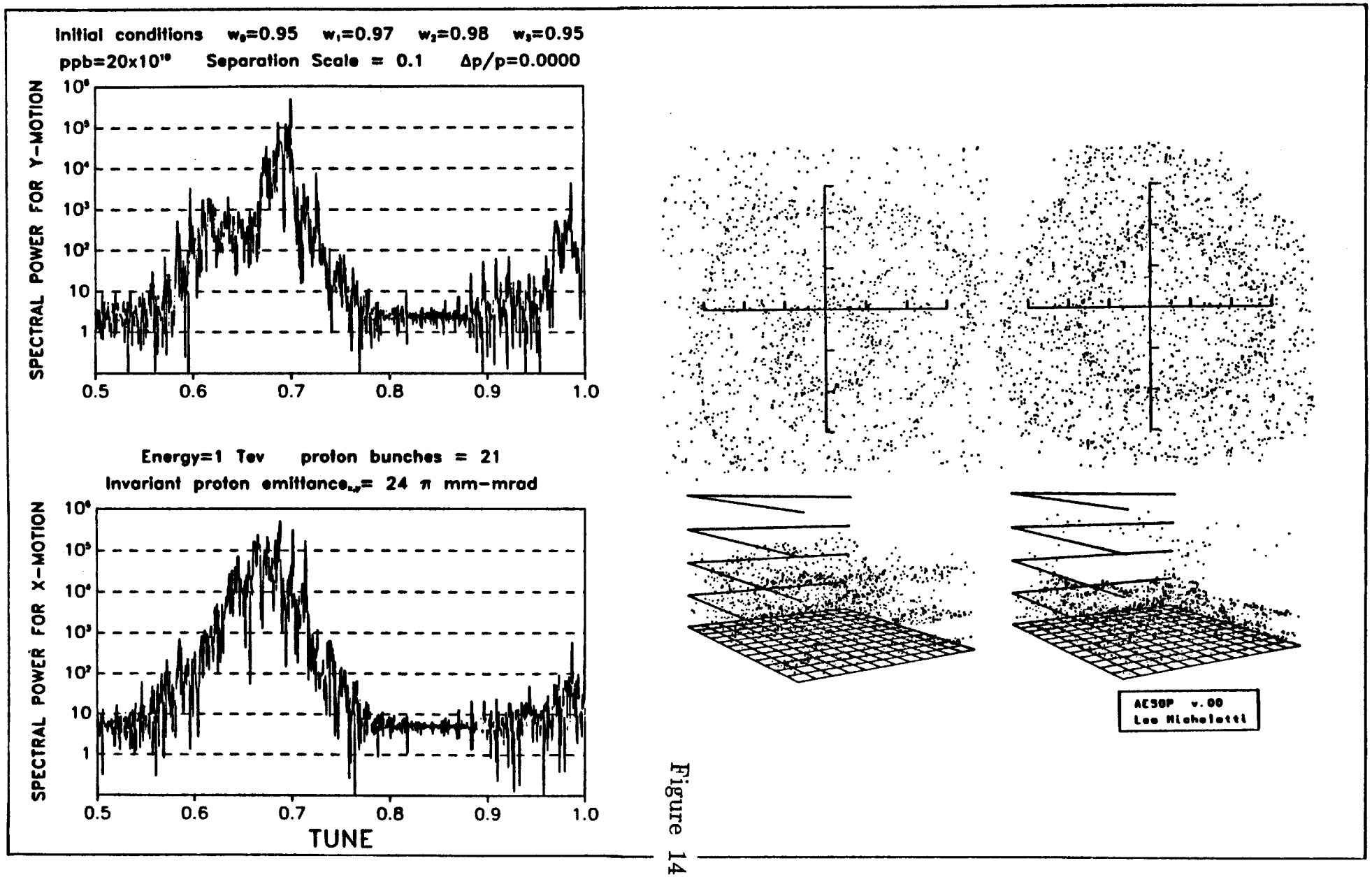
Initial conditions w_0=0.95 w_1=0.97 w_2=0.98 w_3=0.95
ppb=20x10^{10} Separation Scale = 0.1 Δp/p=0.0000
SPECTRAL POWER FOR Y-MOTION
Energy=1 Tev proton bunches = 21
Invariant proton emittance$_{x,y}$= 24 π mm-mrad
SPECTRAL POWER FOR X-MOTION
TUNE
AESOP v.00
Lee Michelotti

Figure 14(b)

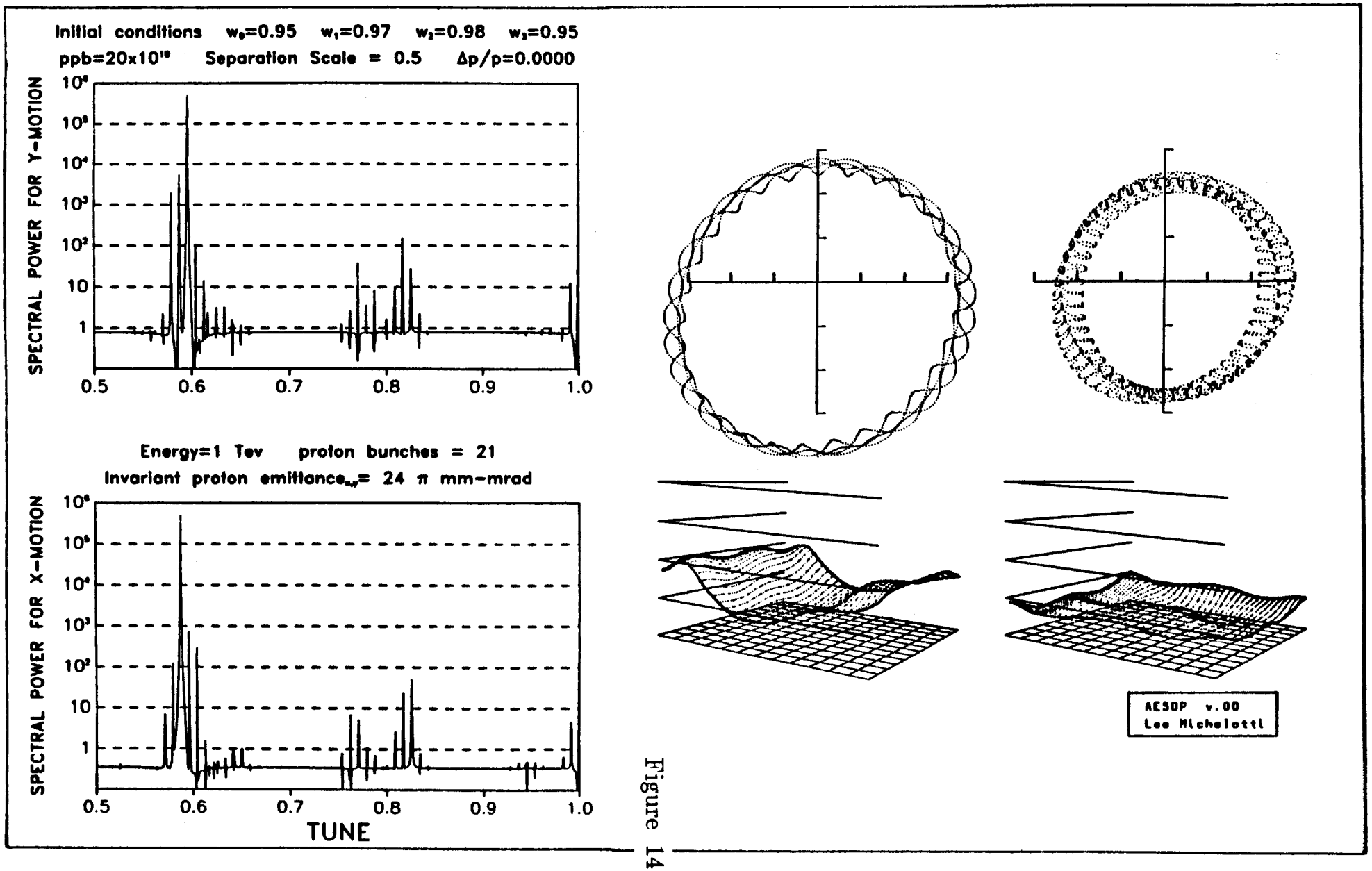
Initial conditions w_0=0.95 w_1=0.97 w_2=0.98 w_3=0.95
ppb=20x10¹⁰ Separation Scale = 0.5 Δp/p=0.0000
SPECTRAL POWER FOR Y-MOTION
Energy=1 Tev proton bunches = 21
Invariant proton emittance = 24 π mm-mrad
SPECTRAL POWER FOR X-MOTION
TUNE
AESOP v.00
Lee Michelotti

Figure 14(c)

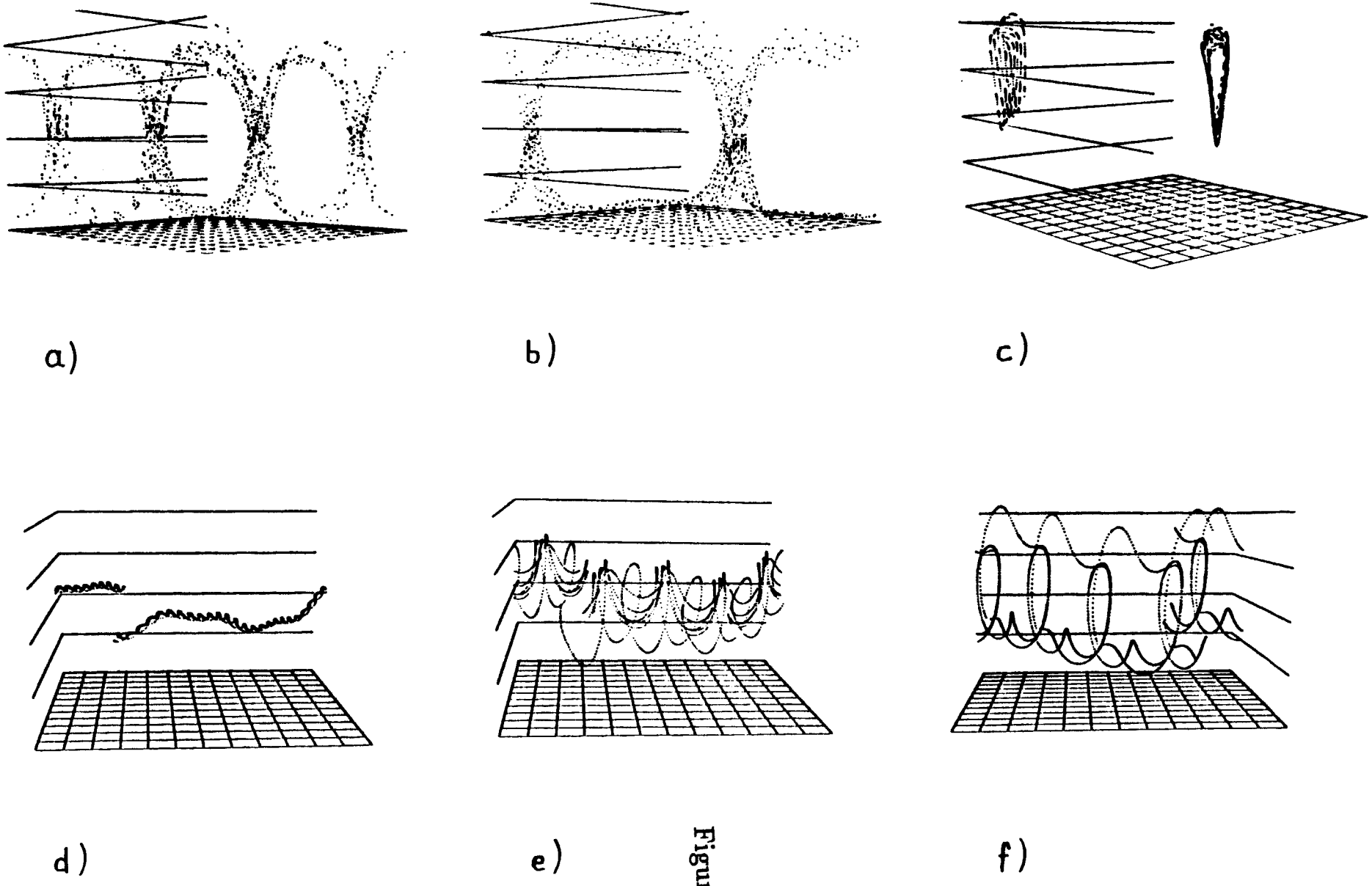

Figure 15

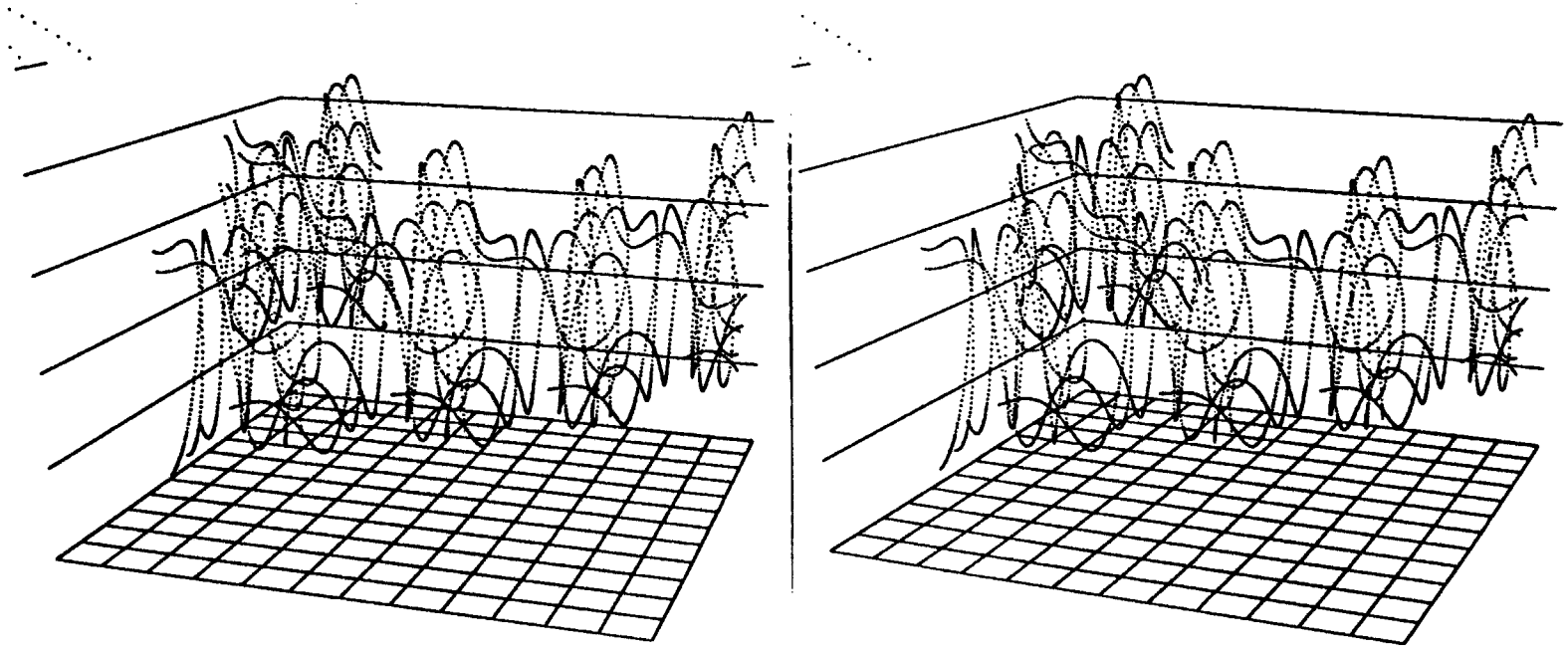

Stereo view; tangled orbit 11/29/88 44

Figure 16

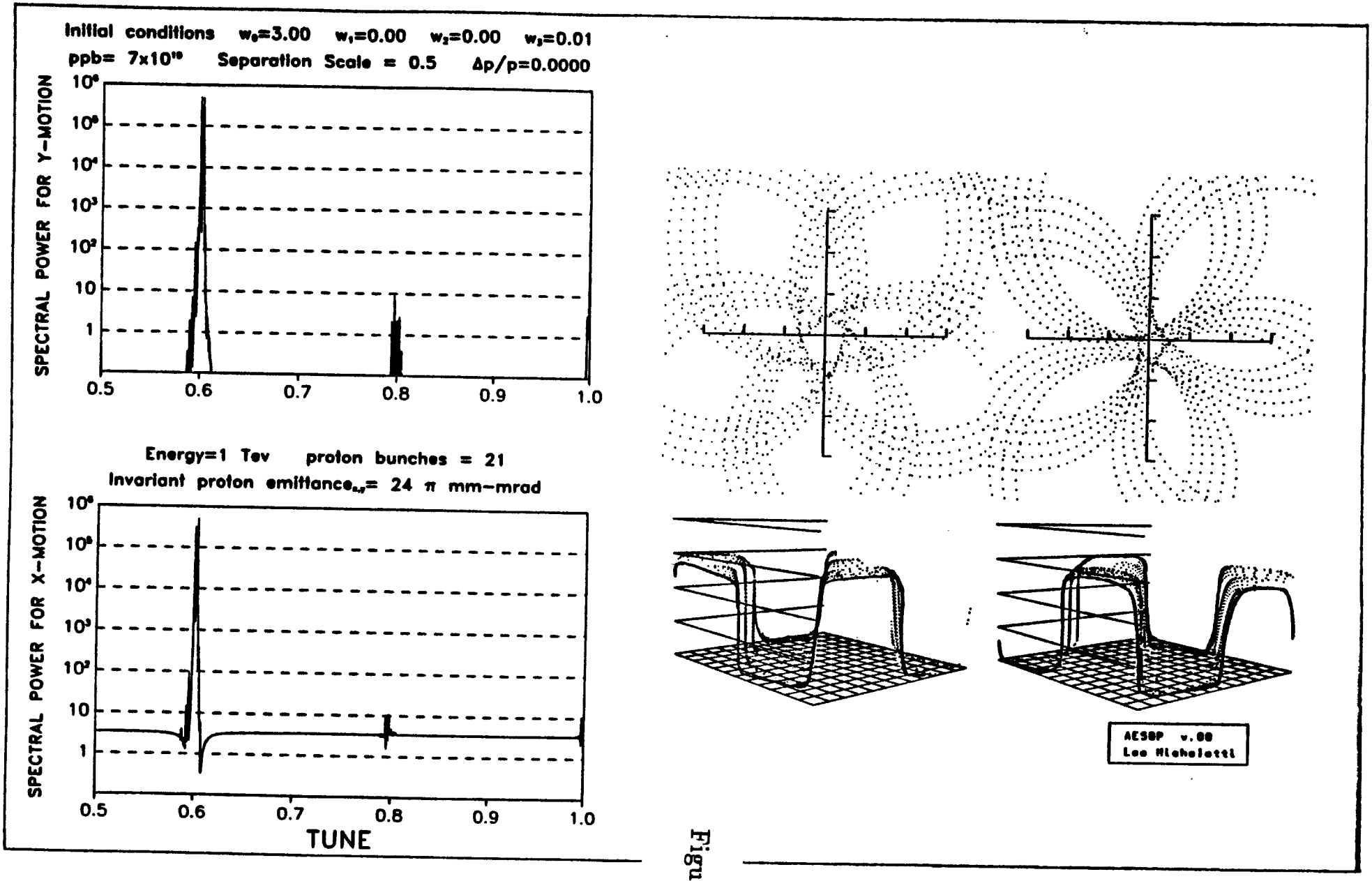
Initial conditions w_0=3.00 w_1=0.00 w_2=0.00 w_3=0.01
ppb= 7x10¹⁰ Separation Scale = 0.5 Δp/p=0.0000
SPECTRAL POWER FOR Y-MOTION
Energy=1 Tev proton bunches = 21
Invariant proton emittance$_{x,y}$= 24 π mm-mrad
SPECTRAL POWER FOR X-MOTION
TUNE
AESOP v.00
Lee Michelotti

Figure 17